Structural, Morphometric and Immunohistochemical Study of the Rabbit Accessory Olfactory Bulb

Running title: Rabbit Accessory Olfactory Bulb

Paula R. VILLAMAYOR [a], Jose Manuel CIFUENTES [a], Luis QUINTELA [b], Ramiro BARCIA [c], Pablo SANCHEZ-QUINTEIRO [a]

[a] Department of Anatomy, Animal Production and Clinical Veterinary Sciences. Faculty of Veterinary. University of Santiago de Compostela. Lugo, Spain.
[b] Department of Animal Pathology. Faculty of Veterinary. University of Santiago de Compostela. Lugo, Spain.
[c] Department of Biochemistry and Molecular Biology. Faculty of Veterinary. University of Santiago de Compostela. Lugo, Spain.

Correspondence:
Dr. Pablo Sanchez-Quinteiro, Department of Anatomy, Animal Production, and Clinical Veterinary Sciences. Faculty of Veterinary, University of Santiago de Compostela, Av Carballo Calero s/n, 27002 Lugo, Spain.

e-mail: pablo.sanchez@usc.es

Orcid IDs:

Paula R. VILLAMAYOR: 0000-0002-7361-7795
Jose Manuel CIFUENTES: 0000-0001-9169-9651
Luis QUINTELA: 0000-0002-0580-1216
Ramiro BARCIA: 0000-0002-7943-3452
Pablo SANCHEZ-QUINTEIRO: 0000-0002-9891-4817

ACKNOWLEDGEMENTS

The authors thank COGAL SL (Pontevedra, Spain) for providing most of the animals employed in this study. Special thanks are due to Alejandro García MD, DVM for his artistic drawing of the AOB topography. We also thank Professor Ignacio Salazar, for his support and constant encouragement during his fruitful period as Head of the Department of Anatomy.

FUNDING

This work was supported by a University of Santiago de Compostela grant [1551-8179] to PSQ.

ABSTRACT

The accessory olfactory bulb (AOB) is the first neural integrative centre of the vomeronasal system (VNS), which is associated primarily with the detection of semiochemicals. Although the rabbit is used as a model for the study of chemocommunication, these studies are hampered by the lack of knowledge regarding the topography, lamination, and neurochemical properties of the rabbit AOB. To fill this gap, we have employed histological stainings; lectin labelling with *Ulex europaeus* (UEA-I), *Bandeiraea simplicifolia* (BSI-B4), and *Lycopersicon esculentum* (LEA) agglutinins; and a range of immunohistochemical markers. Anti-G proteins Gαi2 / Gαo, not previously studied in the rabbit AOB, are expressed following an anteroposterior zonal pattern. This places Lagomorpha among the small group of mammals that conserve a double-path vomeronasal reception. Antibodies against olfactory marker protein (OMP), growth-associated protein-43 (GAP-43), glutaminase (GLS), microtubule-associated protein-2 (MAP-2), glial-fibrillary-acidic protein (GFAP), calbindin (CB), and calretinin (CR) characterise the strata and the principal components of the BOA, demonstrating several singular features of the rabbit AOB. This diversity is accentuated by the presence of a unique organisation: four neuronal clusters in the accessory bulbar white matter, two of them not previously characterized in any species (the γ and δ groups). Our morphometric study of the AOB has found significant differences between sexes in the numerical density of principal cells, with larger values in females, a pattern completely opposite to that found in rats. In summary, the rabbit possesses a highly developed AOB, with many specific features that highlight the significant role played by chemocommunication among this species.

KEYWORDS: accessory olfactory bulb, vomeronasal system, immunohistochemistry, rabbits, morphometry, sexual dimorphism.

INTRODUCTION

Chemical communication is one of the primary forms of communication that living beings use among themselves and with the environment (Wyatt, 2003). The primary systems responsible for the detection of chemical molecules are the main olfactory system (MOS) and the accessory olfactory system (AOS) (Brennan & Zufall, 2006; Swaney & Keverne, 2009; Pardo-Bellver et al. 2017). Olfaction represents the most primitive sense in the majority of mammalian species and plays a crucial role during sexual and social behaviours, as well as spatial orientation (Brown, 1985; Slotnick, 2001; Ihara et al. 2013). The main olfactory epithelium (MOE) receptors have evolved to detect a broad range of odorants, while vomeronasal organ (VNO) receptors have evolved to detect limited groups of ligands, primarily intraspecific pheromonal cues but also a variety of heterospecific cues from sympatric competitors and predators (Grus et al. 2005; Ben-Shaul et al. 2010; Isogai et al. 2011). However, the AOS is well-known to be capable of recognising other chemical signals, and the MOS is capable of detecting pheromones (Boehm, 2006; Mandiyan et al. 2005; Yoon et al. 2005). This functional synergy between these two systems is likely associated with their structural similarities. Although the anatomical features between the two systems are well-distinguished (Wysocki, 1979; Halpern & Martinez-Marcos, 2003), they are not completely morphologically independent, as demonstrated by not only the presence of vomeronasal receptors expressed in the olfactory mucosa and viceversa (Rodriguez et al. 2000, in humans; Sam et al. 2001 and Trinh & Storm, 2003, both in mice), but also by their overlapping projections within the same subregions of the rat amygdala (Pro-Sistiaga et al. 2007).

In mammals, rabbits represent one of the best models for studying chemocommunication (González-Mariscal et al. 2016). Rabbits remain the only mammal species in which a mammary pheromone (MP; 2-methylbut-2-enal), has been fully characterised (Schaal et al. 2003). MP is released by lactating females to awaken rabbit

70 neonates and initiate the nipple-sucking reflex. The fact that the receptors involved in the MP
71 detection have still not been identified reflects the lack of knowledge on the anatomical and
72 physiological basis of all the structures involved in rabbits chemocommunication. Although in
73 four days old rabbits the detection of MP has been linked to the MOB by cFos studies (Charra
74 et al. 2012), a similar approach at postnatal day 0 (Schneider et al. 2016) did not find activation
75 in either the MOB or the AOB. These contradictory results remark the necessity of structural
76 and morphofunctional studies of the chemosensory systems in rabbits, especially regarding
77 the vomeronasal system, very crucial for reproduction and maternal behaviour in such close
78 related species as rodents (Keverne, 2002). A necessary first step is to characterize the almost
79 unexplored adult rabbit AOB.

80 Pheromones play a pivotal role in rabbits and can act as cues for submissive or
81 dominant behaviours (Melo & González-Mariscal, 2010). Because rabbits are often prey
82 animals, olfaction is an essential sense for the detection of danger, predators, and potential
83 mates (Apfelbach et al. 2005, Ben-Shaul et al. 2010). Recently, rabbits have increasingly been
84 introduced as domesticated forms of livestock and pets, and in many areas of the world, they
85 are part of daily life, in the forms of food, clothing and pets. Although the behavioural cues and
86 reproductive features of rabbits have been investigated for decades (Verga et al. 2007;
87 Szendrő et al. 2012), the techniques employed in these studies were primarily environment
88 enrichment (Szendrő et al. 2013) or the induction of hormonal changes to enhance
89 reproduction (Vega et al. 2012). Instead, studying pheromones appears to be a suitable
90 method for improving the welfare of rabbits, reducing their stress levels and increasing their
91 reproductive efficiency (Bouvier & Jacquinet, 2008).

92 In Rodentia, the vomeronasal system (VNS) and its association with pheromone
93 detection have been studied extensively, using morphological (Halpern, 1987; Meisami &
94 Bhatnagar, 1998; Holy, 2018), molecular (Mombaerts, 2004; Zufall & Leinders-Zufall, 2007;

Isogai et al. 2011; Trouillet at al. 2019), and electrophysiological techniques (Mohrhardt et al. 2018), and these studies have demonstrated that the VNS play a pivotal role in species survival. Given the phylogenetic proximity between Lagomorpha (consisting of two families: Leporidae and Ochotonidae) and Rodentia, greater knowledge of the VNS may demonstrate the importance of chemocommunication in rabbits, and establish how both systems, MOB and AOB, can work together during communication between individuals of the same species.

Unfortunately, rabbit physiological and behavioural information has not been examined in concert with an exhaustive structural study of the VNS. The vomeronasal system is composed of the VNO, the AOB and the vomeronasal amygdala, and all of these are linked to each other through the vomeronasal nerves and tracts.

The primary structural features of the rabbit VNO have recently been studied in depth, showing a highly developed organ, with many specific morphological features and considerable immunohistochemical reactivity, suggesting that the organ is highly functional (Villamayor et al. 2018). However, there remains a lack of information regarding the structural and immunohistochemical properties of the AOB. Only a few studies are available, showing low-power histological images that appear to show a laminar structure (Segovia et al. 2006; Meisami & Bhatnagar, 1998; Schneider et al. 2018), in addition to a few studies that have employed monoclonal antibodies against glycoconjugates (Mori, 1987; Mori et al. 1987).

Although the AOB generally presents a laminar structure located caudally to the MOB, the AOB can have significant structural, phylogenetic, and species-specific variations among mammals (Meisami & Bhatnagar, 1998). The AOB is completely developed in some species, such as rodents (Rodriguez et al. 1999), marsupials (Jia & Halpern, 2004), and prosimians (Skeen & Hall, 1977). In other species, such as the African elephant (Ngwenya et al. 2011), West Indian manatee (Mackay-Sim et al. 1985) and humans (Trotier et al. 2000), the AOB is absent or has not yet been identified, whereas in dogs (Salazar et al. 2013), mink (Salazar et al.

1998), and some bats (Frahm & Bhatnagar, 1980), the AOB is present but appears to be poorly developed.

In the present work, a morphological and immunohistological analysis of the rabbit AOB was performed. We aimed to investigate the general features of the rabbit AOB at both the macroscopic and microscopic levels, to further our understanding of the anatomy of this component of the VNS. Various tissue dissection and microdissection techniques were used, as well as general and specific histological stainings and lectin-histochemical labelling. We studied 3 lectins: *Ulex Europaeus* agglutinin (UEA), a specific marker for the vomeronasal pathway in several species (Salazar et al. 2013); *Bandeiraea simplicifolia* isolectin B4 (BSI-B4), a specific marker for the VNS in both rats (Salazar & Sanchez-Quinteiro, 1998) and opossums (Shapiro et al. 1995); and *Lycopersicon esculentum* agglutinin (LEA), a specific marker for both olfactory systems.

In addition, an exhaustive immunohistochemical study was performed. We employed a wide variety of antibodies, for the first time, to examine the rabbit olfactory bulb. Among these antibodies, antibodies against G proteins are especially useful, as Gαi2 and Gαo subunit expression has been associated with the functional activity of the vomeronasal receptor families V1R and V2R, respectively (Shinohara et al. 1992; Jia & Halpern 1996). The primary neuronal elements of the bulb were characterised using microtubule-associated protein 2 (MAP-2) and α-glutaminase (GLS) antibodies. The neuronal growth and maturation were demonstrated by examining anti-growth-associated protein 43 (GAP-43), and anti-olfactory marker protein (OMP) staining, respectively. Antibodies against calbindin (CB) and calretinin (CR), which are both calcium binding proteins, recognised proteins expressed in large quantities in both olfactory bulbs. Finally, an antibody against glial fibrillary acidic protein (GFAP) was employed as a marker of astrocytes and ensheathing cells.

The examination of the neuronal organisation of the rabbit AOB was completed with the microscopical study of the neuronal clusters encased within the accessory bulbar white matter, immediately beneath the AOB internal cellular layer (ICL). Following their first description by Ramón y Cajal (1904) these sub-bulbar structures have received very little attention. They only have been studied comprehensively in rats, mice, and guinea pigs by Larriva-Shad (2012) who linked them with the transitional zone of the AOB. Our findings reveal that these sub-bulbar structures are more complexly organised in rabbits than has previously been described for other mammalian AOBs. With this study, we have addressed the existing knowledge gap regarding the structural and immunohistochemical characterisation of the first neural integrative centre of the VNS in rabbits.

MATERIAL & METHODS

For the structural and immunohistochemical study ten adult healthy rabbits of both sexes aged from at least 3.0 months to 1 year old. For the morphometric study twelve adult healthy rabbits, six of each sex, aged 70 days old. All of them were provided by an abattoir and were commercial Hyplus hybrid (Grimaud Frères, France). The rabbits were humanely sacrificed by electric shock under current legislation [Council Regulation (EC) 1099/2009], and the heads were separated from the carcasses in the slaughtering line. In addition, the intact heads from two adult BALB/c mice bred and euthanized for research in the Department of Pharmacy of the same faculty were kindly donated to the authors. They were used as a positive control in the immunohistochemical protocols. All procedures followed the guidelines for housing and handling provided by the Bioethical Committee of the University of Santiago de Compostela, and conformed to European legislation (EU directive 2010/63/EU) and Spanish legislation (RD 53/2013).

Two of the rabbit heads were dissected fresh for macroscopic studies of the anatomy of the vomeronasal system. The remaining heads were dissected only superficially and rapidly fixed by immersion in either 10% buffered formalin (Fr) or Bouin's fixative (Bn). In the latter case, after 24 h, the specimens were transferred to 70% ethanol. We performed all the experiments in both fixers, and overall we found better results using Bn than Fr, apart from Tolivia and Bielschowsky stainings, which required Fr fixation.

After fixation, the olfactory bulbs (OBs) were completely dissected out for processing. Paraffin wax embedding was the most commonly performed type of inclusion. The OBs were cut into sagittal and transverse serial 5-8 µm sections for the examination of the AOB topography. The sections were stained with Nissl, Tolivia and Bielschowsky stainings. Immunohistochemical and lectin-histochemical stainings were performed in paraffin embedded sections. Calcium-binding proteins immunohistochemistry was additionally

180 performed in free-floating sections. To perform the latter, after their fixation by immersion in
181 either Fr or Bn, two unembedded bulbs were cryoprotected by immersion overnight at 4 °C in
182 30% sucrose in 0.1 M phosphate-buffer (PB) and cut into 40-µm sagittal sections using a
183 freezing microtome.

184 *Tolivia protocol*

185 The sections were mordanted for 1 h in 2.5% $(SO_4)_2FeNH_4$. The myelin staining solution
186 was freshly prepared as follows: 5 ml of 20% hematoxylin plus 10 ml of 1% Li_2CO_3 in 50 ml of
187 50% ethanol. The slides were placed in the solution for 2.5 hours. After 3 x 5 min washes, the
188 samples were stained for 5 min in the following solution: 0.2% pyronine in 20% formaldehyde.
189 Finally, the samples were dehydrated, cleared and mounted (Tolivia et al. 1988).

190 *Bielschowsky's silver stain protocol*

191 Dewaxed and hydrated slides were stained in 20% silver nitrate in dark at 37 °C for 30
192 min. After 2 x 5 min washes in distilled water, concentrated ammonia was added to the silver
193 solution drop by drop until the precipitate formed was completely dissolved. Samples were
194 then incubated in this solution for 15 min at 37 °C in dark followed by 2 x 10 min 0.1 %
195 ammonia washes. The developer solution is made up of 20 ml formaldehyde 10%, 100 ml
196 distilled water, 0.5 g citric acid, and 2 drops of nitric acid. Such solution was added to the initial
197 silver solution and then the samples were rinsed in it for 10 min. The samples were washed
198 again with ammonia and placed for 1 min in 5% sodium thiosulfate ($Na_2S_2O_3$). In some cases,
199 the sections were counterstained with pyronin. Finally, the slides were washed in distilled
200 water, dehydrated, cleared and mounted.

201 *Lectin histochemistry protocol*

202 The lectins LEA and BSI-B_4 were obtained as biotin conjugates from Vector (Vector
203 Laboratories, Burlingame, CA, USA) and used as follows. (i) First, the sections were treated

with 3% hydrogen peroxide in distilled water to quench endogenous peroxidase activity. (ii) Incubation for 30 min at room temperature with 2% bovine serum albumin (BSA) in 0.1 M Tris buffer (pH 7.2). (iii) The sections were incubated overnight at room temperature in the biotinylated lectins diluted in 0.5% BSA. (iv) The next day, the slides were incubated for 1.5 hours at room temperature in Vectastain ABC reagent (Vector Laboratories, Burlingame, CA, USA). (v) Peroxidase activity was visualized by incubation in a solution containing 0.05% 3,3-diaminobenzidine (DAB) and 0.003% H_2O_2 in 0.2 M Tris–HCl buffer (pH 7.6) for 5 min. DAB was the chromogen and developed into a brown precipitate. Controls were run without lectin and with preabsorption of lectin by an excess amount of the corresponding sugar. Finally, the slides were dehydrated with alcohols, cleared in xylene and coverslipped.

Additionally, we used unconjugated UEA-I from Vector (Vector Laboratories, Burlingame, CA, USA). The steps (i) and (ii) were the same as above. (iii) The samples were incubated for 1 h at room temperature with the lectin UEA-I diluted in 0.5% BSA. (iv) Then, they were washed for 3 x 5 min in PB. (v) For 12 h, the samples were incubated with an immunoglobulin (Ig) against UEA conjugated to peroxidase (Dako, Denmark). (vi) The samples were washed in PB and (vii) they were finally incubated in DAB solution and dehydrated and mounted as above.

Controls were run both without lectin and with preabsorption of lectin by an excess amount of the corresponding sugar. None of these sections showed positive staining.

Immunohistochemical protocol for paraffin-embedded tissue

All primary antibody incubations were performed at 4 °C temperature while the secondary antibodies were incubated at room temperature. Both were kept in a humid chamber during the entire procedures. Unless otherwise stated, all washing steps consisted of three successive 5 min rinses in PB.

The sections were quenched in 3% H_2O_2 for 15 min. Next, non-specific binding was blocked for 30 minutes with either 2.5% horse normal serum of the ImmPRESS reagent kit Anti-mouse IgG / Anti-rabbit IgG (Vector Laboratories, Burlingame, CA, USA) or 2% BSA for 30 minutes (Table 1). ImmPRESS is a non-avidin–biotin polymer-based immunohistochemistry detection system which avoids the background staining due to endogenous biotin or avidin (Ramos-Vara & Miller, 2006). The sections were then incubated overnight with the primary antibody. The next day the samples previously blocked with the ImmPRESS kit were incubated for 20 minutes with either the corresponding ImmPRESS VR Polymer HRP Anti-Rabbit IgG Reagent or the Anti-Mouse IgG Reagent (Vector Laboratories). Those samples blocked in 2% BSA were instead washed and incubated in biotinylated secondary antibody raised against goat-IgG and after three washes they were incubated in Vectastain ABC reagent for 1.5 h. In all cases, after rinsing in 0.2 M Tris–HCl buffer (pH 7.6) for 10 min, the sections were finally developed using DAB as chromogen as we described for the lectin histochemical labelling, and then dehydrated and mounted.

Double Immunohistochemical protocol for paraffin-embedded tissue

For double immnunostaining, a sequential twice-repeated enzyme-labeled method was employed (Hasui et al. 2003). Between both immunolabellings, the sections were subjected to treatment with 0.1 M glycine solution (pH 2.2) for 5 min. To select the most suitable dye to visualize the immunoreaction, both DAB and Vector VIP Peroxidase Substrate Kit (SK-4600, Vector Laboratories) were combined exchanging their order. Using first DAB and then VIP was the optimal combination for our immunostaining.

Immunohistochemical protocol for free-floating sections of unembedded tissue

Firstly, we performed an antigen retrieval step, to expose the protein epitopes. The freezing microtome sections were placed at 80 °C for 30 min in 10 mM buffer, pH 6.0. From that point, the immunohistochemistry was similar to that followed in slide-mounted sections.

In all the immunohistochemical procedures, samples for which the primary antibody was omitted were used as negative controls, without obtaining labelling or unspecific background in any case. In addition, as positive controls, we replicated the immunohistochemical procedure with mouse tissues known to express the proteins of interest, obtaining the expected positive results.

Morphometric and stereological study

The OB of the animals used in this part of the study, 12 rabbits, six from each sex, were immediately extracted and preserved in 10% formalin buffered. After paraffin embedding the whole OBs were serial sectioned at 7 µm in the sagittal plane. The processing protocol was carefully standardized so that the samples treated followed an identical regime.

Morphometry

To estimate the volume of the AOB and MOB subdivisions, the Cavalieri principle was used. After serial sectioning of the whole OB, every 17th section for the AOB and every 40th for the MOB were selected for analysis. To ensure that the estimator is unbiased the placement of the first section plane was chosen randomly. Ten to thirteen sections were sampled from each MOB, and ten to fourteen from each AOB following this systematic random manner. The sections were photomicrographed at low magnification (5X objective for AOB, and 1,20X for the MOB) and the boundaries and perimeters of each layer were manually outlined and digitized using a graphic pad (Intuos, Wacom) linked to a microcomputer.

After filling each layer with a pseudocolor (different gray levels for each layer), the total area of each region was determined using ImageJ software (ImageJ 1.52a, National Institutes of Health, USA). The total volume of each region was obtained by multiplying the sum of the areas of the individual profiles of each region by the number of sections measured and the distance between two sections. This distance was obtained from the product of the section thickness (7 µm) by the sampling interval.

A correction for tissue shrinkage during processing was applied (Mouton, 2002). It required determining the change in area from the original unfixed state, to the sample on which the morphometry was performed. It corresponded to 1.8643.

Stereology

The number of cells for unit of volume was directly estimated by the physical dissector (Sterio, 1984). After applying the dissectors over the photomicrographs of the 'reference sections' they were compared with their pairs ('look up' sections). To do this, 2 micrographs were made (20× objective) of each paired section. According to the findings obtained from a pilot study, the first chosen section and its adjacent section, were separated by a distance of 7 µm. The distance between the pair of sections must be about 30-40% of the average height of the object of interest

Once the same histological area was located in both paired slices, the template with the dissectors (3-4 by section) was superposed on the reference image and counted the number of cells (Q-) of the reference image that fell within the counting frame without touching the forbidden lines (straight lines) and did not appear in the "look up" image. Finally, the number of dissectors (P) used was counted. The mean numerical density of cells was estimated using the following formula:

$$N_v = \frac{1}{\Delta x \cdot \Delta y \cdot h} \cdot \frac{\sum Q^-}{\sum P}$$

Where $\Delta x \cdot \Delta y$ is the area of the dissector; h: the distance between paired sections of the dissector (in this case, 7 µm); $\Sigma Q-$: sum of neurons counted according to the dissector, in every "volume section"; ΣP: sum of dissectors used to measure the cells.

The number of sections studied varied from 10 to 13, depending on the bulb. In each section from 2-3 zones were studied and 2-4 dissectors were accounted for each.

Acquisition of images and digital processing

The digital images were captured with a Karl Zeiss Axiocam MRc5 digital camera paired to a Zeiss Axiophot microscope. Figures 1b-d, 3-9 and 11-13 were then adjusted for fine-tune of the brightness and contrast and balance levels, applied to the whole image, by using Adobe Photoshop CS4 (Adobe Systems, San Jose, CA, USA). In any case, no specific feature within an image was enhanced, moved or introduced. In addition, those figures which were made up of several photographs (figure 5a-b, 12a, 13a-d) were merged with an image-stitching software (PTGui Pro) and then cropped and resized by using Photoshop. These mosaics are presented as supplementary material (Suppl. Fig. 7-8).

RESULTS

Anatomical and histological study

The primary structures of the VNS are shown both macroscopically and microscopically in Fig. 1. The inner sensory neuroepithelium of the VNO is enclosed in a cartilaginous tubular structure located in the ventral part of the nasal septum (Fig. 1a, b). The nerve fibres of the vomeronasal nerves link the VNO to the brain (Fig. 1a, c). The AOB is the first relay station of the VNS. In rabbits, the AOB is located caudal and dorsally to the elongated main olfactory bulb (MOB) and ventral to the frontal lobe (Fig. 1d). The thin amyelinic branches of the vomeronasal nerve are difficult to visualise macroscopically along their pathway through the submucosa of the nasal septum, intermingled with the olfactory nerves (Fig. 2a). After passing through the cribriform plate, the branches converge into a unique nerve that courses along the medial segment of the MOB (Fig. 2b), ending in a small elevation in the caudalmost part of the bulb, partially covered by the frontal lobe (Fig. 2c, d).

The primary microscopical features of the AOB were studied using Nissl, Tolivia, and Bielschowsky staining techniques. Nissl staining showed a large, semi-oval, and well-laminated AOB, in both sagittal and transversal sections (Fig. 3a-d). The thickness and the sharpness of boundaries among the layers were neat. The outermost layer of the AOB is formed by the fibres of the vomeronasal nerves, which spread over the surface to form a definite fibre layer and then turn inward to shape the glomeruli. The glomeruli of the AOB are smaller than those of the MOB, and they are densely packed. Although the organisation of the glomeruli in the AOB appears to be more diffuse than the organisation of the glomeruli in the MOB (Fig. 3e, f), Bielschowsky staining showed a supraglomerular organisation (Fig. 4c), which was not noticeable with Nissl staining. Whereas in the MOB the whole perimeter of the glomeruli is delimited by periglomerular cells (Fig. 4b), in the AOB, these cells are primarily concentrated along the border between the glomerular and ICL layers, forming a very narrow band (Fig. 4a).

In order to describe the deep layers of the AOB we have adhered to the nomenclature proposed by Larriva-Sahd (2008) who avoids the customary use of terms taken from the description of the MOB. Neither the main cells of the AOB are mitral in shape nor is there an authentic plexiform layer. For that reason, we will use, following Larriva-Sahd, the term external cellular layer (ECL) for what has usually been called mitral-tufted layer, ICL for the granular layer, and principal cells instead of mitral cells.

Instead of a typical monolayer of mitral-like cells, the principal cells of the AOB are scattered along the broad ECL, which extends from the glomerular layer (GlL) to the internal cellular layer (ICL) (Fig. 3e, 4f). Both Nissl and Tolivia staining of the AOB principal cells (Fig. 4d, e, h) showed that they are not as characteristically mitral in shape as the mitral cells of the MOB (Fig. 4f). Instead, they show a variable morphology, with three main types: large principal cells, rounded cells, and tufted cells (Fig. 4d, e). Large principal cells have big ovoid nucleus with patent nucleolus and a large soma; rounded cells possess a smaller rounded nucleus, and tufted cells remember to the tufted cells of the MOB. The tufted cells are intensely stained by Nissl and Tolivia stainings (Fig. 4h), have a triangular shape and present a prominent primary dendrite. They are often concentrated in groups (Fig. 4e).

The ICL forms the deepest layer of the AOB. This layer contains medium-sized granule cells, grouped into islets, which are overlaid by the myelinic efferent fibres of the AOB, as demonstrated by both the Tolivia and Bielschowsky methods (Fig. 4f, 5a, b). These axonal fibres, which project from the ECL, constitute the contribution of the AOB to the dorsal peduncle of the lateral olfactory tract (LOT), which in rabbits courses under the ICL (Fig. 5c).

Immunohistochemical and lectin-histochemical study

Most of the immunohistochemical markers used in this study stained the superficial layers of the AOB, following different patterns. The immunostaining using the anti-GFAP antibody shows the glial components. The labelling was restricted to the vomeronasal nerve

362 layer (VNL). Despite the lack of astrocytes, positive immunostaining of the processes from
363 vomeronasal ensheathing cells was observed, surrounding and subdividing the neuropil (Fig.
364 6a-c). Moreover, in all of the specimens studied, there was a noticeable concentration of
365 astrocytes external to the pial basement membrane that surrounds the AOB (Fig. 6a, d).

366 The presence of olfactory marker protein (OMP), an olfactory neuron maturation
367 marker, in both the AOB and the MOB was demonstrated by the binding of the anti-OMP
368 antibody to the superficial layers of the whole bulb. The staining was constricted to the nerve
369 and GlLs of both bulbs.

370 The expression of antibodies against G proteins, Gαi2 and Gαo subunits, has been
371 associated with the functional activity of the main vomeronasal receptor families V1R and V2R,
372 respectively. Double and single immunolabelling of the G protein subunits Gαi2 and Gαo
373 showed that the expression patterns of both proteins in the superficial layers of the AOB
374 follow a zonal segregation pattern (Fig. 7a-d). The antibody against Gαi2 stained only the
375 anterior half of the VNL-GlL layers of the AOB, whereas the posterior half of both layers was
376 not stained at all (Fig. 7a, c). The boundary between the stained anterior segment and the
377 unstained posterior segment is sharp and clear. The antibody against Gαo stained the
378 posterior half of the VNL-GlL layers. The anterior half of the nerve layers was not stained,
379 although the glomeruli appeared to be partially stained (Fig. 7b, d). The staining of these latter
380 glomeruli corresponds with the dendrites from neurons in the underlying layers of the AOB.
381 The boundaries between the posterior and anterior segments of the VNL-GlL layers are also
382 clear and sharp. Unlike the differential staining observed for the VNL-GlL layers of the AOB, the
383 staining for Gαo is relatively uniform in other regions of the brain, including the ECL and ICL
384 layers of the AOB and all of the layers in the MOB.

385 The anti-GAP-43 staining reflected a high level of axonal growth. The immunolabelling
386 appears to be more intense in both the superficial and internal cellular layers of the AOB (Fig.

7f). In the superficial layers, GAP-43 staining revealed the zonal organisation of the AOB, with stronger labelling in the anterior zone than in the posterior zone, defining both areas very neatly. Moreover, in the MOB, anti-GAP-43 stained the internal plexiform layer (IPL) more strongly than the external plexiform layer (EPL) (Fig. 7h). This pattern was conserved in the AOB, establishing a distinction between the superficial and deep ECLs (Fig. 7f).

We used lectin histochemical techniques to characterize the glycoconjugates expression in the superficial layers of the rabbit AOB. The expression of such glycoconjugates varies among species allowing, in some cases, to characterize specifically both olfactory systems. Among the three lectins used, the N-acetylglucosamine-specific LEA (Fig. 7e), and the α-galactose-specific BSI-B_4 (Fig. 7g) stained the VNL and GlL of the AOB, without defining antero-posterior zonation. Both of these lectins also stained the corresponding layers of the MOB. The L-fucose-specific UEA did not stain any part of the olfactory bulb.

AOB principal cells were characterised not only with histological staining but also by using antibodies against GLS and MAP-2. The former antibody labelled the somas of mitral cells in the MOB (Fig. 8c) and principal cells of the AOB, mostly those with elongated somas but also large principal cells (Fig. 8d). No type of AOB principal cells were immunolabelled with the antibody to GABA.

Anti-MAP-2 antibody is a useful marker for the dendritic trees of mitral/principal cells. The MAP-2 immunoreactivity infiltrated all of the glomeruli in the AOB, but did not intermingle with the axons of the VNL, as shown by the double immunohistochemical labelling with MAP-2 and Gαi2 antibodies (Fig. 8a, b). The immunolabelling was very dense in the ECL but did not affect the mitral cell somas. In the granule cells of the ICL, MAP-2 immunolabelled the spherical cell bodies and the processes that lead towards the superficial regions of the AOB.

The calcium binding proteins CR and CB are valuable markers of neuronal subtypes. The antibodies against both of them labelled the AOB. The staining was primarily concentrated

in the neuropil of the superficial and middle layers (Fig. 9a, b). The periglomerular (PG) cells were not immunopositive, either in cryostat free-floating sections (Fig. 9a) or in paraffin-embedded sections (Fig. 9b). The absence of CB and CR PG cells in the AOB contrasts with their presence in the MOB, where the glomeruli are found to be neatly delineated by the immunopositive PG cells (Fig. 9d, e). Granule cells are labelled by both the antibodies against CR and anti-CB.

Neuronal clusters in the accessory bulbar core white matter

Nissl-stained serial sagittal sections of the bulb showed four distinct cellular clusters that contained pyramidal-like neurons parallel to the base of the AOB. These nuclei were encased in the accessory bulbar white matter of the LOT, immediately beneath the ICL. They follow an ordered topographical pattern that is demonstrated in Fig. 10. Two of these nuclei were located in the caudal half of the AOB, with one located medially and one located laterally. The other two nuclei were located at the level of the anterior third of the AOB, in a similar fashion, with one located medially and the other located laterally. The caudal nuclei correspond to what have been termed the α and β groups of the anterior olfactory nucleus (AON) (Valverde et al., 1989). The α group is situated in the medial aspect of the bulb, whereas the β cluster is located closer to the lateral surface. The two rostral nuclei are described here for the first time. One is located medially, while the other is located laterally. According to the criteria used to name the caudal nuclei, we have named these nuclei the γ and δ groups, respectively.

In all cases, the Nissl sagittal stainings (Fig. 11, 12a, b, 13) showed that the nuclei contain large, deeply stained, oval and polygonal cells. The presence of the four nuclei was also confirmed in our Nissl transverse serial sections (Fig. 13). Pyronin and Bielschowsky stains confirmed that the clusters are encapsulated by the thick fibres of the dorsal LOT (Fig. 12c, d).

436 The immunohistochemical study showed that the nuclei are composed of GLS-immunoreactive
437 cells (Fig. 12e).

438 *Morphometric and stereological study*

439 There were no sex differences in the volume of the nervous, glomerular, external
440 cellular, and internal cellular of the AOB (see Table 2 and Fig.14). Additionally, in order to
441 compare the relative volumes of the glomerular layer in both bulbs, a similar morphometric
442 study was done in the MOB. There were again no sex differences in the layer volumes of the
443 MOB except in the deep granule cell layer (Suppl. Material. Table 1 Figure…[EI3]).

444 The density study (number of neurons per volume unit) of the ECL found significant
445 differences by sex in the neuronal density in the ECL of the AOB. Females showed a greater
446 number of neurons per volume than male rabbits ($t = 2.72$, $P < 0.01$) (Fig. 15).

DISCUSSION

Several developments during the last decades have greatly contributed towards the improving our understanding of the VNS in mammals. Regrettably, these contributions have not been based on the precise knowledge of the neuroanatomical basis of this system, except in laboratory rodents (Takami & Graziadei, 1991; Keverne, 2002; Larriva-Sahd, 2008; Barrios et al. 2014) and opossums (Halpern & Martínez-Marcos, 2003) and, beyond mammals, the singular case of the garter snakes (Martínez-Marcos et al., 2002).

There are significant structural, phylogenetic, and species-specific variations among AOB locations, shapes, sizes and morphologic differentiation and development patterns. The AOB can either be perfectly developed (Rodriguez et al. 1999), poorly differentiated (Nakajima et al. 1998), or entirely absent (Ngwenya et al. 2011) depending on the species.

Although rabbits have become a model for the study of chemocommunication in mammals (Schaal et al. 2003, Schneider et al. 2018), there remains a lack of morphological and immunohistochemical information regarding the structural features of their AOBs. Amusingly, the term “accessory olfactory bulb” was coined by Gudden (1870) after his macroscopic observations of the rabbit olfactory bulb. However, apart from the early microscopic observations reported by Ramón y Cajal (1904), only a few studies feature the AOB more than incidentally (Segovia et al. 2006; Meisami & Bhatnagar, 1998; Mori et al. 1987; Schneider et al. 2018).

We have found that the adult rabbit has a fully developed AOB, in terms of size, topography, cell density, as well as the sharpness of the boundaries between AOB layers and its definite antero-posterior zonal organization. In addition, the shape, size, distribution and arrangement of neurons are all well-developed in the rabbit AOB. These features in rabbits can be compared to those found in marsupials, such as opossums (Jia & Halpern, 2004),

prosimians, such as *Tupaia* (Skeen & Hall, 1977), and rodents, such as mouse, rat, and capybara (Salazar et al. 2006; Larriva-Sahd, 2008; Suarez et al. 2011b).

To discuss the primary morphological features of the AOB, we have organised the discussion into three sections, moving from superficial to deep: the VNL and GlL; the ECL; and the ICL. We have followed the nomenclature proposed by Larriva-Sahd (2008) whose more significant changes are the introduction of two new layers, an ECL joining the former external granular layer (EGL), mitral-tufted layer (MTL) and EPL, and an ICL replacing the internal granule layer (IGL).

Superficial layers: Vomeronasal nerve and glomerular layers

The most superficially located layer (the vomeronasal nerve layer) consists of thick bundles of unmyelinated vomeronasal nerve fibres that open into the deeper GlL. AOB glomeruli consist of an acellular neuropil. When comparing MOB and AOB glomeruli, the appearance of AOB glomeruli is very loose because of their smaller sizes and densely packed arrangement. Additionally, in the MOB, the whole perimeter of the glomeruli is delimited by PG cells, whereas in the AOB these cells are concentrated along the border between the GlL and plexiform layers, forming a very narrow band. This organisation is quite similar to that found in the mouse AOB (Salazar et al. 2006; Yokosuka, 2012).

The glomerular map in the AOB appears to be more complex than that in the MOB. Wagner et al. (2006) found in mice that inputs from neurons expressing closely related V1Rs intermingle within shared domains of the AOB. At the same time, individual principal cells extend dendrites to glomeruli associated with different, but likely closely related, V1Rs. These features of the glomerular organization were showed in the rabbit AOB by Mori (1983) who reconstructed a whole dendritic tree of a of single mitral/tufted cells and verified that it emits two to four stem dendrites that make terminal arborizations within from three to seven the glomeruli.

The nervous fibres in the VNL are enclosed by numerous ensheathing cells, which promote the regenerative abilities of VNL receptor neurons (Chehrehasa et al. 2014). GFAP is a commonly used marker for these cells in mammals and other vertebrates (Lazzari et al. 2016; Smithson & Kawaja, 2009). Anti-GFAP immunostaining allowed us to identify the nuclei and the profuse arborisations of these cells in the rabbit AOB.

Both superficial layers (VNL and GlL) showed different labelling patterns for immunostaining against Gαi2, Gαo, GAP-43, OMP, CB and CR and for histochemical staining with two of the three lectins, BSI-B_4 and LEA.

The vomeronasal and olfactory receptors are linked to receptor-activated heterotrimeric G proteins (composed of Gα and Gβ/Gγ subunits), which represent important components of the cell signalling cascade in VNO neurons (Dulac & Torello, 2003). Thus far, the Gαi2 and Gαo subunits have been associated with the two primary vomeronasal receptor families: V1R and V2R, respectively (Shinohara et al. 1992; Jia & Halpern 1996).

Analyses of G protein distribution, using immunolabelling in the AOBs of several mammals, have shown that V1R-Gαi2 neurons project their axons towards the glomeruli located in the AOB rostral region, whereas the V2R-Gαo neurons project towards glomeruli in the caudal region. This segregated projection within the AOB has been observed in Rodentia (Mouse: Jia & Halpern, 1996; rat: Shinohara et al. 1992; degu: Suarez & Mpodozis, 2009; and capibara: Suarez et al. 2011b), Marsupialia (Opossum: Halpern et al. 1995) and Afrosoricida (Lesser hedgehog tenrec: Suarez et al. 2009). However, it is not a common feature among mammals, and the Gαo pathway is absent in several orders, including Artyodactila (Goat: Takigami et al. 2000), Peryssodactila (Horse: Takigami et al. 2004), Carnivora (Dog: Salazar et al. 2013; cat: Salazar & Sanchez-Quinteiro, 2011), Insectivora (Musk shrew: Takigami et al. 2004), Primates (Marmoset: Takigami et. al, 2004), Hyracoidea (African cape hyrax: Suarez et al. 2011a) and some Rodentia (Squirrels: Suarez et al. 2011a).

Here, we provide the first report of both Gαi2 and Gαo proteins being expressed in the AOB of Lagomorpha. Our previous immunohistochemical contributions to the VNO (Villamayor et al. 2018) showed that in the rabbit vomeronasal sensory epithelium, both Gαi2 and Gαo expressing neurons coexist. However, they do not organise following a zonal pattern of distribution: Gαi2 labels a subpopulation of apical cells, whereas Gαo labels a broader pattern over the whole neuroepithelium. These results contrasted with the well-defined apical Gαi2 and basal Gαo pattern found in species such as opossum (Halpern et al. 1995), mouse (Barrios et al. 2014), and rat (Jia & Halpern, 1996). Therefore, we addressed the following questions: does the AOB contain both typical Gαo and Gαi2 subclasses of vomeronasal neurons, are these subclasses of neurons segregated in the AOB, and do they follow the same ill-defined pattern observed in the VNO?

Our single and double immunohistochemical labelling of G proteins in the AOB has shed light on the distribution of the vomeronasal receptor subclasses in the rabbit AOB. Both antibodies not only discriminate two zones of the AOB but they also follow an anterior-posterior zonation pattern. These immunohistochemical results likely extrapolate to the effective expression patterns of the two families of receptors, V1R and V2R, as occurs in rodents. Thus, Lagomorpha align with the small group of mammalian orders that have two pathways of functional vomeronasal receptors. This molecular finding likely reflects the importance of vomeronasal chemocommunication in rabbits.

Our observations of the G protein expression patterns in the rabbit AOB agrees with those obtained by Mori et al. (1987) in the same species using monoclonal antibodies against lactoseries carbohydrates. They found that the R4B12 antibody labelled a subgroup of fibres that ended in the AOB rostrolateral glomeruli, whereas the R5A10 antibody recognised a complementary subgroup of VNNs that terminated in the AOB caudomedial portion. Although they were unable to determine the functional significance of this heterogeneity at the time,

546 this heterogeneity is now recognised to represent the zonation established by Gαo and Gαi2
547 proteins and the patterns determined by some glycoconjugates, which have been observed
548 either through the histochemical labelling of lactoseries carbohydrates (Jessell et al. 1990) or
549 through the lectin histochemical identification of carbohydrate moieties (Shapiro et al. 1995).

550 Therefore, we also studied the carbohydrates moieties in the rabbit AOB by employing
551 the three lectins most commonly used in both the MOS and the VNS. The functional
552 significance of the sugar residues detected by lectin histochemistry has been suggested to
553 include neurite outgrowth, synaptic plasticity, signal transduction and/or cell-cell interactions
554 (Kinzinger et al. 2005). The affinities with which different lectins bind to the AOB vary among
555 taxa and even among closely related species.

556 For instance, UEA has been considered to be a specific marker of the vomeronasal
557 pathway (VNO, VNN and AOB) in adult mice (Kondoh et al. 2017; Salazar et al. 2001), whereas
558 the lectin BSI-B_4 has been recognised as an excellent specific marker of the VNS in both rats
559 (Salazar & Sanchez-Quinteiro, 1998) and opossums (Shapiro et al. 1995). However, we found
560 that UEA failed to produce labelling in the rabbit AOB and VNNs. This negative pattern has also
561 been found in sheep (Salazar et al. 2000) and Korean roe deer (Park et al. 2014), whereas in
562 other species, such as rats (Salazar & Sanchez-Quinteiro, 1998) and pigs (Salazar et al. 2000),
563 UEA labels both the MOS and the AOS.

564 In rabbits, BSI-B_4 labels both the AOB and the MOB and therefore cannot be
565 considered to be a VNS-specific marker. Furthermore, we also studied the LEA labelling pattern
566 in rabbits, and we found that this lectin stains the GlL and nervous layer of both the AOB and
567 the MOB, with a highly conserved pattern, as has been described in a wide range of species,
568 including mouse, sheep, pig, and deer (Salazar et al. 2000 & 2001; Park et al. 2014).

569 Together, these results suggest that glycoconjugates play an important role in primary
570 olfactory and vomeronasal organisation; however, the bases of their detailed expression

patterns in every species remain still poorly understood, demonstrating that the diversity among mammalian VNS structures is not only morphological but also neurochemical, physiological, and behavioural.

The antibody against GAP-43 unexpectedly revealed the zonal organisation of the rabbit AOB. Although the anti-GAP43 antibody immunolabelled the entire AOB, we observed that the immunostaining was much stronger within the anterior zone, whereas the posterior zone showed weaker labelling. Thus, both areas were neatly defined. This observation has not been described in any other species for this marker. Additionally, anti-GAP-43 staining established a distinction between the EPL and IPL layers of the MOB and between the superficial and deep ECL of the AOB.

GAP-43 is a useful probe for discriminating between mature axons and regenerating nerve fibres because its levels in newly formed fibres rapidly decline after the fibres reach their targets (Verhaagen et al. 1989; Ramakers et al. 1992). The olfactory system is an area of the adult nervous system that exhibits extensive synaptic plasticity; therefore it is not surprising to find a high level of expression for this marker in the AOB. The zonation observed in rabbits suggests that plasticity is more intense in the anterior AOB than in the posterior AOB.

OMP is another specific marker of the superficial layers of the whole bulb. OMP staining in rabbits was restricted to the nervous strata and the GlLs, and was weaker in the AOB than in the MOB. This pattern of labelling is similar to that identified by our group in the neuroepithelium of the rabbit VNO (Villamayor et al. 2018), which was very profuse in both the apical dendrites and axons of the vomeronasal sensory neurons.

Specific immunohistochemical staining for OMP was detected in mature vomeronasal and olfactory receptor-expressing neurons (Farbman & Margolis, 1980; Rodewald et al. 2016). Although OMP expression has been studied in a vast range of mammalian VNOs (Dennis et al. 2004 & 2019), the study of its immunoreactivity in the AOB has been restricted to rodents,

596 such as mice, rats, and hamsters (Barrios et al. 2014, Jia & Halpern, 1996, Kream et al. 1984),
597 marsupials, such as opossums (Shnayder et al. 1993), and sheep (Salazar et al. 2007). Although
598 the function of OMP remains unknown, it is thought to be involved in the maturation of
599 olfactory and vomeronasal neurons (Bock et al. 2006). Accordingly, OMP labelling increases
600 with age in both the VNO and the AOB (Verhaagen et al. 1989; Ramakers et al. 1992).

601 Calcium-binding proteins are proteins in large quantities in the olfactory bulb. They
602 have been detected in segregated neuronal populations, allowing the distinction among
603 several neurochemical groups within morphologically homogeneous neuronal types. For the
604 first time, we studied the distribution of CB and CR immunoreactivity in the rabbit AOB. In the
605 superficial layer, entire vomeronasal fibres were immunopositive for both markers, producing
606 positive neuropil staining in all glomeruli. In addition, the whole structure displayed a densely
607 stained neuropil, especially for the CR-immunostained samples. However, the PG cells were
608 not immunopositive for either CR or CB, for paraffin-embedded sections and cryostat free-
609 floating sections.

610 The CR staining pattern observed in rabbits was identical to those observed in rat
611 (Jacobowitz & Winsky, 1991) and opossum (Jia & Halpern 2004) and very similar to that found
612 in hedgehog (Briñón et al. 2001), identifying in the latter species a small population of
613 immunopositive cell bodies surrounding the glomeruli without identifying cell processes.

614 CB labelling in the superficial layers of the AOB showed more significant interspecies
615 differences than CR labelling. For instance, in rats (Porteros et al. 1995) and opossums (Jia &
616 Halpern, 2003 & 2004) the neuropil was much less stained than in rabbits; however, in both
617 cases, rats and opossums, some individual glomeruli are immunostained and accompanied by
618 isolated positively stained PG cells.

619 **External cellular layer (ECL)**

The Nissl histological staining of the rabbit AOB showed a broad and diffuse arrangement of the principal cells. This arrangement does not allow the distinction of the three layers typically found in the MOB: MCL, EPL, and IPL. Therefore, it is more realistic to consider the MCL and the plexiform layers as a single structure, the ECL, similar to that described in the rat and mouse AOB (Larriva-Shad, 2008; Martín-López et al. 2012).

Interestingly, we have observed that the immunohistochemical labelling of GAP-43 in the rabbit could be a useful probe for discriminating both plexiform layers. Principal cells do not express this antibody, either in the soma or in the dendrites, whereas anti-GAP-43 immunostains the plexiform neuropil, following a zonal profile. This profile can easily be observed in the rabbit MOB, where the IPL is strongly marked by the GAP-43-antibody, whereas the EPL is more lightly stained. This pattern makes sense because most of the axons are concentrated in the IPL. This pattern is conserved in the AOB, although the border between the layers is not as neat as in the MOB; however, we can conclude that the existence of two plexiform layers in the AOB is far from a theoretical concept.

Although projecting cells in the AOB share similarities with mitral cells in the MOB, their somata are rarely mitral shaped, and their connectivity is different (Mori, 1983). Thus, the term mitral should be avoided. Accordingly, we adopt the nomenclature proposed by Larriva-Sahd (2008) who described in rat three types of principal cells: large principal cells, round projecting cells and tufted cells. The first of these is by far the most numerous in the rat's olfactory bulb. The rabbit AOB presents a similar cellular diversity in its principal cells, with three cell types morphologically comparable to those present in rats. However, large principal cells do not predominate as much as it happens in rodents (Takami & Graziadei, 1991; Larriva-Sahd, 2008). The positive immunohistochemical labelling observed for the GLS antibody, demonstrates the glutamatergic nature of the rabbit AOB principal cells, similar to the pattern observed for rodents (Quaglino et al. 1999).

Anti-MAP-2 is a useful marker for mitral cell dendritic trees (Dehmelt & Halpain, 2005) and it is absent from axons (Bernhardt & Matus, 1984). Anti-MAP-2 staining revealed a very dense immunolabelling in the ECL layer of the rabbit AOB, corresponding with the profuse dendritic trees of principal cells. The MAP-2 immunolabelling also revealed the global contribution of these cells to glomeruli, similar to what has been observed in the mouse AOB (Salazar et al. 2006).

However, in the rabbit AOB the soma of the principal cells was not labelled by anti-MAP-2, whereas in the mouse AOB, principal cells somas were stained by this antibody. This contradictory finding could be explained due to the slightly different molecular structure of the protein that binds differently to IgG, but more likely reflects specific variations in the distributions of the protein within the soma. AOB principal cells were also negative for calcium-binding protein immunostaining in the rabbit, similar to what has been observed for opossum, rat and mouse (Jacobowitz & Winsky, 1991; Jia & Halpern, 2004).

Internal cellular layer: Granule cells - White matter α-group of the Anterior olfactory nucleus

The granule cells of the rabbit AOB have the same general morphology as those found in the MOB. They are not compactly amassed together, as usually occurs in the AOB of most species (Meisami & Bathnagar, 1998). Instead, the granule cells are grouped into islets, which are very neatly defined by the myelinic fibres of the LOT when visualised using the Bielschowsky method. Both the granule cells and the neuropil are labelled by antibodies against MAP-2, CR, and CB antibodies. The immunolabelling results demonstrate spherical cell bodies and processes that arise and extend toward the superficial regions of the AOB. This pattern is similar to that described in rats, mice, hedgehogs and opossums (Porteros et al. 1995; Jia & Halpern, 2004; Briñón et al. 2001).

669 The axonal fibres projecting from the ECL constitute the contribution of the AOB to the
670 dorsal LOT. In rabbits these fibres pass through the AOB towards the dorsal LOT which courses
671 under the ICL. This trait has been used as a phylogenetic indicator of common ancestry in
672 mammals (Switzer et al. 1980). This trait is present in most of the Euarchontoglires, a clade of
673 mammals recently defined based on DNA sequence analyses (Murphy et al. 2001) and
674 comprised of five groups (Rodentia, Lagomorpha, Dermoptera, Scandentia, and Primatea). In
675 contrast, marsupials, carnivores and ungulates, these fibers pass under the AOB, as observed
676 for the tammar wallaby (Schneider et al. 2012), cat (Salazar & Sanchez-Quinteiro, 2011) and
677 roe deer (Park et al. 2014). Our finding confirms the hypothesis established by Schwitzer et al.
678 that whereas Rodentia has the trait of dorsal LOT fibers passing through the accessory
679 olfactory formation, Lagomorpha represent an intermediate stage in the evolution of this trait.

680 The deepest layer of the rabbit AOB has an additional striking feature that has received
681 very little attention: the presence, parallel to its ventral segment, of a series of pyramidal-like
682 neuronal clusters that are neatly delimited by the myelinic fibres of the dorsal LOT. One such
683 cluster was first described by Ramón y Cajal in the guinea pig (1904), although he was not able
684 to assign it any function. Lohman (1963) studied these clusters in the guinea pig using Nissl
685 staining, assuming that they belonged to the pars rostralis of the AON. Valverde et al. (1989),
686 in their study on the hedgehog AON, described the presence two similar small cell populations
687 in the bulbar portion of the AON. These populations were respectively located in the medial
688 and lateral sections of the dorsal extension of the pars externa of the AON and they were
689 referred to as the α and β groups of the AON. Larriva-Sahd (2012) studied the α-group in rats,
690 mice, and guinea pigs, and reported that the dendrites of these pyramidal-like cells organise
691 into a bundle that ascends to the trigone bounded by the edges of the olfactory limb, the AOB
692 and the dorsal section of the AON. Accordingly, these islands are likely to be functionally
693 related to the sensory qualities detected by both the MOB and AOB.

The only description of this type of cluster in rabbits was reported by Moses Wharton Young (1936), who in his study of the non-cortical centres of the telencephalon of the rabbit, included both groups in a schematic transverse drawing of the caudal part of the olfactory bulb. They were described in the text as circular patches of cells in the medial and lateral extremes of the pars dorsalis of the AON. Undoubtedly, these patches are the rabbit equivalents of the α and β groups of the AON that were described by Valverde et al. (1989).

Our sagittal and transverse serial sections of several specimens of the rabbit AOB demonstrate that, in addition to the α and β clusters, the rabbit possesses two clusters topographically related to the anterior AOB, one of which is located medially, whereas the other is found laterally. Following the Valverde criteria, we have named them the γ and δ groups. The anterior positioning of these additional groups makes it very unlikely that they are associated with the AON, supporting the observations of Larriva-Sahd (2012), who associated the α group with the second order processing of olfactory and vomeronasal information. Future studies should address the roles played by these unique neuronal formations.

Morphometrical study

Although we have not found qualitative histological and immunohistochemical differences between sexes in the rabbit AOB, the morphometric study pointed to the existence of sexual differences. We found that the volume of the female AOB layers was slightly larger than that found in males, apart from the case of the glomerular layer. But, in each case the differences were not statistically significant. Comparing this result with that obtained by Segovia et al. (1987) in their morphometric study of the vomeronasal system of the rabbit, both studies found a similar nonsignificant tendency.

However, our stereologic study has determined a statistically significant difference between sexes regarding the numerical density of the principal cells within the ECL. The females have greater numerical density values than the males. In this case, although Segovia et

al. observed significant sexual differences in the total number of cells in the mitral cellular layer, the sexual difference values become statistically non-significant when these values were adjusted according to the volume of each layer. Our study, carried out with the same number of animals from both sexes but with a greater number of sections and dissectors, has allowed us not only to confirm the trends found by Segovia et al. (1987) but also to conclude that a statistically significant sexual dimorphism exists in the numerical density of the principal cells of the external cell layer.

Our contribution and the study by Segovia et al. (1987), taken together, make a strong case for the conclusion that the female rabbit AOB presents higher morphometric values than the male. However, in a previous research on the AOB of the rat (Guillamón & Segovia, 1997), they found a significant sexual dimorphism, but in this case with greater morphological values in males. There is no explanation for these species differences in the expression of sexual dimorphism, although we agree with Guillamón & Segovia that they are probably a consequence of the reproductive, behavioural, and physiological traits of each species. In that regard, it should be borne in mind that female rabbits are reflex ovulators while female rats are spontaneous ovulators, and that the sexual and maternal behaviours also differ between the species.

The existence of two divergent patterns in species as close as the rat and the rabbit raises a warning about the risk of extrapolating to other species the findings obtained in rodents on the sexual dimorphism of the brain.

After this exhaustive characterisation of the rabbit AOB, we conclude that the adult rabbit possesses a differentiated and sexually dimorphic AOB, featuring many specific particularities at both the structural and functional levels. These results highlight the significance of chemocommunication in this species, and further anatomical studies that include the connectivity and functional properties of the principal cells of the AOB, as well

744 other parts of the VNS, namely, the vomeronasal amygdala, should be performed. Moreover,
745 given that chemocommunication is especially important during the early stages of life (Schaal
746 et al. 2003), developmental anatomical studies examining the maturity of the rabbit VNS
747 during prenatal and early postnatal stages are also necessary.

COMPLIANCE OF ETHICAL STANDARDS

Conflict of interest

The authors declare that the research was conducted in the absence of any commercial or financial relationships that could be construed as a potential conflict of interest.

Ethical approval

All procedures performed in this study involving living animals were in accordance with the ethical standards of the Institutional Animal Care Committee of the Universidad de Santiago de Compostela under procedure number MR110250.

Informed consent

No human subject was used in this study.

REFERENCES

Apfelbach R, Blanchard CD, Blanchard RJ et al (2005) The effects of predator odors in mammalian prey species: a review of field and laboratory studies. *Neurosci Biobehav Rev* **29**, 1123-44.

Barrios AW, Nuñez G, Sanchez-Quinteiro P et al (2014) Anatomy, histochemistry, and immunohistochemistry of the olfactory subsystems in mice. *Front Neuroanat* **8**, 63.

Ben-Shaul Y, Katz LC, Mooney R et al (2010) In vivo vomeronasal stimulation reveals sensory encoding of conspecific and allospecific cues by the mouse accessory olfactory bulb. *PNAS* **107**, 5172-7.

Bernhardt R, Matus A (1984) Light and electron microscopic studies of the distribution of microtubule-associated protein 2 in rat brain: a difference between dendritic and axonal cytoskeletons. *J Comp Neurol* **226**, 203-21.

Bock P, Rohn K, Beineke A et al (2006) Site-specific population dynamics and variable olfactory marker protein expression in the postnatal canine olfactory epithelium. *J Anat* **215**, 522–535.

Boehm U (2006) The vomeronasal system in mice: from the nose to the hypothalamus- and back! *Semin Cell Dev Biol* **17**, 471-9.

Bouvier AC, Jacquinet C (2008) Pheromone in rabbits. Preliminary technical results on farm use in France. WRSA Congress –Proceedings.

Brennan PA, Zufall F (2006) Pheromonal communication in vertebrates. *Nature* **444**, 308-15.

Briñón JG, Weruaga E, Crespo C et al (2001) Calretinin-, neurocalcin-, and parvalbumin-immunoreactive elements in the olfactory bulb of the hedgehog (Erinaceus europaeus). *J Comp Neurol* **429**, 554-70.

Brown RE (1985) Effects of social isolation in adulthood on odor preferences and urine-marking in male rats. *Behav Neural Biol* **44**, 139-43.

Charra R, Datiche F, Casthano A et al (2012) Brain processing of the mammary pheromone in newborn rabbits. *Behav Brain Res* **226**, 179-188.

Chehrehasa F, Ekberg JA, St John JA (2014) A novel method using intranasal delivery of EdU demonstrates that accessory olfactory ensheathing cells respond to injury by proliferation. *Neurosci Lett*. **563**, 90-5.

785 **Dehmelt L, Halpain S (2005)** The MAP2/Tau family of microtubule-associated proteins. *Genome*
786 *Biol* **6**, 204.
787 **Dennis JC, Smith TD, Bhatnagar KP et al (2004)** Expression of neuron-specific markers by the
788 vomeronasal neuroepithelium in six species of primates. *Anat Rec* **281**, 1190-200.
789 **Dennis JC, Stilwell NK, Smith TD et al (2019)** Is the mole rat vomeronasal organ functional?
790 *Anat Rec*, doi:10.1002/ar.24060.
791 **Dulac C, Torello AT (2003)** Molecular detection of pheromone signals in mammals: from genes
792 to behaviour. *Nat Rev Neurosci* **4**, 551-62.
793 **Farbman AI, Margolis FL (1980)** Olfactory marker protein during ontogeny:
794 immunohistochemical localization. *Dev Biol* **74**, 205-215.
795 **Frahm HD, Bhatnagar KP (1980)** Comparative morphology of the accessory olfactory bulb in
796 bats. *J Anat* **130**, 349-65.
797 **Guillamón A, Segovia S (1997)** Sex differences in the vomeronasal system. *Brain Res Bull* **44**,
798 377-82.
799 **González-Mariscal G, Caba M, Martínez-Gómez M et al. (2016)** Mothers and offspring: The
800 rabbit as a model system in the study of mammalian maternal behavior and sibling interactions. *Horm*
801 *Behav* **77**, 30-41.
802 **Grus WE, Shi P, Zhang Y et al (2005)** Dramatic variation of the vomeronasal pheromone
803 receptor gene repertoire among five orders of placental and marsupial mammals. *PNAS* **102**, 5767–
804 5772.
805 **Gudden B (1870)** Experimental untersuchungen über das peripherische und centrale
806 nervensystem. *Arch Psychiatr Nervenkr* **11**, 693–723.
807 **Halpern M (1987)** The organization and function of the vomeronasal system. *Annu Rev Neurosci*
808 **10**, 325-62.
809 **Halpern M, Martínez-Marcos A (2003)** Structure and function of the vomeronasal system: an
810 update. *Prog Neurobiol* **70**, 245-318.
811 **Halpern M, Shapiro LS, Jia C (1995)** Differential localization of G proteins in the opossum
812 vomeronasal system *Brain Res* **677**, 157-61.

Hasui K, Takatsuka T, Sakamoto R et al (2003) Double autoimmunostaining with glycine treatment. *J Histochem Cytochem* **51**, 1169-76.

Holy TE (2018) The Accessory Olfactory System: Innately Specialized or Microcosm of Mammalian Circuitry? *Annu Rev Neurosci* **41**, 501-525.

Ihara S, Yoshikawa K, Touhara K (2013). Chemosensory signals and their receptors in the olfactory neural system. *Neuroscience* **254**, 45-60.

Isogai S, Si S, Pont-Lezica L et al (2011) Molecular organization of vomeronasal chemoreception. *Nature* **478**, 241-5.

Jacobowitz DM, Winsky L (1991) Immunocytochemical localization of calretinin in the forebrain of the rat. *J Comp Neurol* **304**, 198-218.

Jessell TM, Hynes MA, Dodd J (1990) Carbohydrates and carbohydrate-binding proteins in the nervous system. *Annu Rev Neurosci* **13**, 227-55.

Jia C, Halpern M (1996) Subclasses of vomeronasal receptor neurons: differential expression of G proteins (Gi alpha 2 and G(o alpha)) and segregated projections to the accessory olfactory bulb. *Brain Res* **719**, 117-28.

Jia C, Halpern M (2003) Calbindin D28k immunoreactive neurons in vomeronasal organ and their projections to the accessory olfactory bulb in the rat. *Brain Res* **977**, 261-9.

Jia C, Halpern M (2004) Calbindin D28k, parvalbumin, and calretinin immunoreactivity in the main and accessory olfactory bulbs of the gray short-tailed opossum, *Monodelphis domestica*. *J Morphol* **259**, 271-80.

Keverne EB (2002) Pheromones, vomeronasal function, and gender-specific behavior. *Cell* **108**, 735-8.

Kinzinger JH, Johnson EW, Bhatnagar KP et al (2005) Comparative study of lectin reactivity in the vomeronasal organ of human and nonhuman primates. *Anat Rec* **284**, 550-60.

Kondoh D, Kamikawa A, Sasaki M et al (2017) Localization of α1-2 Fucose Glycan in the Mouse Olfactory Pathway. *Cells Tissues Organs* **203**, 20-28.

Kream RM, Davis BJ, Kawano T et al (1984) Substance P and catecholaminergic expression in neurons of the hamster main olfactory bulb. *J Comp Neurol* **222**, 140–154.

Larriva-Sahd J (2008) The accessory olfactory bulb in the adult rat: a cytological study of its cell types, neuropil, neuronal modules, and interactions with the main olfactory system. *J Comp Neurol* **510**, 309-50.

Larriva-Sahd J (2012) Cytological organization of the alpha component of the anterior olfactory nucleus and olfactory limbus. *Front Neuroanat* 6,23.

Lazzari M, Bettini S, Franceschini V (2016) Immunocytochemical characterisation of ensheathing glia in the olfactory and vomeronasal systems of Ambystoma mexicanum (Caudata: Ambystomatidae). *Brain Struct Funct* **221**, 955-67.

Lohman AHM (1963) The anterior olfactory lobe of the guinea pig. *Acta Anat,* **45**, 9–109.

Mackay-Sim A, Duvall D, Graves BM (1985) The West Indian manatee (Trichechus manatus) lacks a vomeronasal organ. *Brain Behav Evol* **27**, 186-94.

Mandiyan VS, Coats JK, Shah NM (2005) Deficits in sexual and aggressive behaviors in Cnga2 mutant mice. *Nat Neurosci* **8**, 1660-2.

Martín-López E, Corona R, López-Mascaraque L (2012) Postnatal characterization of cells in the accessory olfactory bulb of wild type and reeler mice. *Front Neuroanat* 6:15.

Martínez-Marcos A, Lanuza E, Halpern M (2002) Neural substrates for processing chemosensory information in snakes. *Brain Res Bull* **57**:543-6.

Meisami E, Bhatnagar KP (1998) Structure and diversity in mammalian accessory olfactory bulb. *Microsc Res Tech* **43**, 476-99.

Melo AI, González-Mariscal G (2010) Communication by olfactory signals in rabbits: its role in reproduction. *Vitam Horm* **83**, 351-71.

Mohrhardt J, Nagel M, Fleck D et al (2018) Signal detection and coding in the accessory olfactory system. *Chem Senses* **43**, 667-695.

Mombaerts P (2004) Genes and ligands for odorant, vomeronasal and taste receptors *Nat Rev Neurosci* **5**, 263-78.

Mori K (1983) Mitral cells in the rabbit accessory olfactory bulb: their morphology and response to LOT stimulation. *Soc Neurosci Abst* **9**, 1020.

Mori K (1987) Monoclonal antibodies (2C5 and 4C9) against lactoseries carbohydrates identify subsets of olfactory and vomeronasal receptor cells and their axons in the rabbit. *Brain Res* **408**, 215-221.

Mori K, Imamura K, Fujita SC et al (1987) Projections of two subclasses of vomeronasal nerve fibers to the accessory olfactory bulb in the rabbit. *Neuroscience* **20**, 259-78.

Mouton PR (2002) Principles and Practices of Unbiased Stereology. An Introduction for Bioscientists. Baltimore, MD. John Hopkins University Press.

Murphy WJ, Eizirik E, O'Brien SJ et al (2001) Resolution of the early placental mammal radiation using Bayesian phylogenetics. *Science* **294**, 2348-51.

Nakajima T, Sakaue M, Kato M et al (1998) Immunohistochemical and enzyme-histochemical study on the accessory olfactory bulb of the dog. *Anat Rec* **252**, 393-402.

Ngwenya A, Patzke N, Ihunwo AO et al (2011) Organisation and chemical neuroanatomy of the African elephant (Loxodonta africana) olfactory bulb. *Brain Struct Funct* **216**, 403-16.

Pardo-Bellver C, Martínez-Bellver S, Martínez-García F et al (2017) Synchronized activity in the main and accessory olfactory bulbs and vomeronasal amygdala elicited by chemical signals in freely behaving mice. *Sci Rep* **7**, 9924.

Park C, Ahn M, Lee JY et al (2014) A morphological study of the vomeronasal organ and the accessory olfactory bulb in the Korean roe deer, *Capreolus pygargus*. *Acta Histochem* **116**, 258-64.

Porteros A, Arévalo R, Crespo C et al (1995) Calbindin D-28k immunoreactivity in the rat accessory olfactory bulb. *Brain Res* 689, 93-100.

Pro-Sistiaga P, Mohedano-Moriano A, Ubeda-Bañon I et al (2007) Convergence of olfactory and vomeronasal projections in the rat basal telencephalon. *J Comp Neurol*, **504**, 346-62.

Quaglino E, Giustetto M, Panzanelli P et al (1999) Immunocytochemical localization of glutamate and gamma-aminobutyric acid in the accessory olfactory bulb of the rat. *J Comp Neurol* **408**, 61-72.

Ramakers GJ, Verhaagen J, Oestreicher AB et al (1992) Immunolocalization of B-50 (GAP-43) in the mouse olfactory bulb: predominant presence in preterminal axons. *J Neurocytol* **21**, 853-69.

Ramón y Cajal, S (1904) Corteza Olfativa, in "*Textura del Sistema Nervioso Central del Hombre y los* Vertebrados *Vol.2*", Imprenta y Librería Nicolás Moya, España.

Ramos-Vara JA, Miller MA (2006) Comparison of two polymer based immunohistochemical detection systems: ENVISION+ and ImmPRESS. *J Microsc* **224**, 135-9**.**

Rodewald A, Gisder D, Gebhart VM et al (2016) Distribution of olfactory marker protein in the rat vomeronasal organ. *J Chem Neuroanat* **77**, 19-23.

Rodriguez I, Greer CA, Mok MY et al (2000) A putative pheromone receptor gene expressed in human olfactory mucosa. *Nat Genet* **26**, 18-9.

Rodriguez I, Feinstein P, Mombaerts P (1999) Variable patterns of axonal projections of sensory neurons in the mouse vomeronasal system. *Cell* **97**, 199-208.

Salazar I, Cifuentes JM, Sanchez-Quinteiro P (2013) Morphological and immunohistochemical features of the vomeronasal system in dogs. *Anat Rec* **296**, 146-55.

Salazar I, Sanchez-Quinteiro P (1998) Lectin binding patterns in the vomeronasal organ and accessory olfactory bulb of the rat. *Anat Embryol* **198**, 331-9.

Salazar I, Sanchez-Quinteiro P (2011) A detailed morphological study of the vomeronasal organ and the accessory olfactory bulb of cats. *Microsc Res Tech* **74**, 1109-1120.

Salazar I, Sanchez-Quinteiro P, Alemañ et al (2007) Diversity of the vomeronasal system in mammals: the singularities of the sheep model. *Microsc Res Tec* **70**, 752-62.

Salazar I, Sanchez-Quinteiro P, Cifuentes JM et al (1998) The accessory olfactory bulb of the mink, *Mustela vison*: a morphological and lectin histochemical study. *Anat Histol Embryol* **27**, 297-300.

Salazar I, Sanchez-Quinteiro P, Cifuentes JM et al (2006) General organization of the perinatal and adult accessory olfactory bulb in mice. *Anat Rec* **288**, 1009-25.

Salazar I, Sanchez-Quinteiro P, Lombardero et al (2000) A descriptive and comparative lectin histochemical study of the vomeronasal system in pigs and sheep. *J Anat* **196**, 15-22.

Salazar I, Sanchez-Quinteiro P, Lombardero M et al (2001) Histochemical identification of carbohydrate moieties in the accessory olfactory bulb of the mouse using a panel of lectins. *Chem Senses* **26**, 645-52.

Sam M, Vora S, Malnic B, et al (2001) Odorants may arouse instinctive behaviours. *Nature* **412**, 142.

Schaal B, Coureaud G, Langlois D et al (2003) Chemical and behavioural characterization of the rabbit mammary pheromone. *Nature* **424**, 68-72.

Schneider NY, Datiche F, Coureaud, G (2018) Brain anatomy of the 4-day-old European Rabbit. *J Anat* **232**, 747-767.

Schneider NY, Fletcher TP, Shaw G et al (2012) Goα expression in the vomeronasal organ and olfactory bulb of the tammar wallaby. *Chem Senses* **37**, 567-577.

Schneider NY, Piccin C, Datiche F et al (2016) Spontaneous brain processing of the mammary pheromone in rabbit neonates prior to milk intake*. Behav Brain Res* **313**, 191–200.

Segovia S, Garcia-Falgueras A, Carrillo B et al (2006) Sexual dimorphism in the vomeronasal system of the rabbit. *Brain Res* **1102**, 52-62.

Shapiro LS, Ee PL, Halpern M (1995) Lectin histochemical identification of carbohydrate moieties in opossum chemosensory systems during development, with special emphasis on VVA-identified subdivisions in the accessory olfactory bulb. *J Morphol* **224**, 331-49.

Shinohara H, Asano T, Kato K (1992) Differential localization of G-proteins Gi and Go in the accessory olfactory bulb of the rat. *J Neurosci* **12**, 1275-1279.

Shnayder L, Schwanzel-Fukuda M, Halpern M (1993) Differential OMP expression in opossum accessory olfactory bulb. *Neuroreport* **5**, 193-6.

Skeen LC, Hall WC (1977) Efferent projections of the main and the accessory olfactory bulb in the tree shrew (Tupaia glis). *J Comp Neurol* **172**, 1-35.

Slotnick B (2001) Animal cognition and the rat olfactory system. *Trends Cogn Sci* **5**, 216-222.

Smithson LJ, Kawaja MD (2009) A comparative examination of biomarkers for olfactory ensheathing cells in cats and guinea pigs. *Brain Res* **1284**, 41-53.

Sterio D. C. (1984) The unbiased estimation of number and sizes of arbitrary particles using the disector. *J Microsc* **134**, 127–136e.

Suarez R, Mpodozis J (2009) Heterogeneities of size and sexual dimorphism between the subdomains of the lateral-innervated accessory olfactory bulb (AOB) of Octodon degus (Rodentia: Hystricognathi). *Behav Brain Res* **198**, 306-12.

Suarez R, Fernández-Aburto P, Manger RR et al (2011 a) Deterioration of the Gαo vomeronasal pathway in sexually dimorphic mammals. *PLoS One **6**, e2643*.

Suarez R, Santibáñez R, Parra D et al (2011 b) Share and differential traits in the accessory olfactory bulb of caviomorph rodents with particular reference to the semiaquatic capybara. *J Anat* **218**, 558-65.

Suarez R, Villalón A, Künzle H et al (2009) Transposition and Intermingling of Galphai2 and Galphao afferences into single vomeronasal glomeruli in the Madagascan lesser Tenrec *Echinops telfairi*. *PLoS One* **4**, e8005.

Swaney WT, Keverne EB (2009) The evolution of pheromonal communication. *Behav Brain Res* **200**, 239-47.

Switzer RC 3rd, Johnson JI, Kirsch JA (1980) Phylogeny through brain traits. Relation of lateral olfactory tract fibers to the accessory olfactory formation as a palimpsest of mammalian descent. *Brain Behav Evol* **17**, 339-63.

Szendrő Z, Mikó A, Odermatt M et al (2013) Comparison of performance and welfare of single-caged and group-housed rabbit does. *Animal* **7,** 463–468.

Szendrő Z, Szendrő K, Zotte AD (2012) Management of reproduction on small, medium and large rabbit farms: a review. *Asian-Australas J Anim Sci* **25**, 738-48.

Takami S, Graziadei PP (1991) Light microscopic Golgi study of mitral/tufted cells in the accessory olfactory bulb of the adult rat. *J Comp Neurol* **311**, 65-83.

Takigami S, Mori Y, Ichikawa M (2000) Projection pattern of vomeronasal neurons to the accessory olfactory bulb in goats. *Chem Senses* **25**, 387-393.

Takigami S, Mori Y, Tanioka Y et al (2004) Morphological evidence for two types of Mammalian vomeronasal system. *Chem Senses* **29**, 301-10.

Tolivia J, Tolivia D, Navarro A (1998) New Technique for Differential Staining of Myelinated Fibers and Nerve Cells on Paraffin Sections. *Anat Rec* **222**, 437-440.

Trinh K, Storm DR (2003) Vomeronasal organ detects odorants in absence of signaling through main olfactory epithelium. *Nat Neurosci* **6**, 519-25.

Trotier D, Eloit C, Wassef M et al (2000) The vomeronasal cavity in adult humans. *Chem Senses* **25**, 369-80.

Trouillet AC, Keller M, Weiss J et al (2019) Central role of G protein Gαi2 and Gαi2+ vomeronasal neurons in balancing territorial and infant-directed aggression of male mice. *PNAS* **116**, 5135-43.

Valverde F, López-Mascaraque L, De Carlos JA (1989) Structure of the nucleus olfactorius anterior of the hedgehog (Erinaceus europaeus). *J Comp Neurol* **279**, 581-600.

Vega MD, Barrio M, Quintela LA et al (2012) Evolución del manejo reproductivo en cunicultura. *ITEA* **108,** 172-90.

Verga M, Luzi F, Carenzi C (2007) Effects of husbandry and management systems on physiology and behavior of farmed and laboratory rabbits. *Horm Behav* **52**, 122-9.

Verhaagen J, Oestreicher AB, Gispen WH et al (1989) The expression of the growth associated protein B50/GAP43 in the olfactory system of neonatal and adult rats. *J Neurosci* **9**, 683-91.

Villamayor PR, Cifuentes JM, Fdz.-de-Troconiz P et al (2018) Morphological and immunohistochemical study of the rabbit vomeronasal organ. *J Anat* **233**, 814-27.

Wagner S, Gresser AL, Torello AT et al (2006) A multireceptor genetic approach uncovers an ordered integration of VNO sensory inputs in the accessory olfactory bulb. *Neuron* **50**, 697-709.

Wharton Young M (1936) The nuclear pattern and fiber connections of the non-cortical centers of the telencephalon of the rabbit (*Lepus cuniculus*). *J Comp Neurol* **65**, 295-401.

Wyatt, TD (2003) Pheromones and animal behaviour: Comunication by smell and taste. Cambridge University Press, Cambridge.

Wysocki, CJ (1979) Neurobehavioral evidence for the involvement of the vomeronasal system in mammalian reproduction. *Neurosci Biobehav Rev* **3**, 301-341.

Yokosuka M (2012) Histological properties of the glomerular layer in the mouse accessory olfactory bulb. *Exp Anim* **61**,13-24.

Yoon H, Enquist LW, Dulac C (2005) Olfactory inputs to hypothalamic neurons controlling reproduction and fertility. *Cell* **123**, 669-82.

Zufall F, Leinders-Zufall T (2007) Mammalian pheromone sensing. *Curr Opin Neurobiol* **17**, 483-9.

TABLES

Table 1: Antibodies and lectins used. Species of elaboration, dilutions, manufacturer, catalog number.

Ab/Lectin*	1st Ab species/dilution	1st Ab Catalogue number	2nd Ab species/dilution (Catalogue number)
Anti-Gαo	Rabbit 1:100	MBL 551	ImmPRESS VR HRP Anti-Rabbit IgG Reagent MP-6401-15
Anti-Gαi2	Rabbit 1:100	Sta Cruz Biotechnology SC-7276	ImmPRESS VR HRP Anti-Rabbit IgG Reagent MP-6401-15
Anti-OMP	Goat 1:400	Wako S44-10001	Horse 1:250 Vector BA-9500
Anti-MAP2	Mouse 1:200	Sigma M4403	ImmPRESS VR HRP Anti-Mouse IgG Reagent MP-6402-15
Anti-GAP43	Mouse 1:800	Sigma G9264	ImmPRESS VR HRP Anti-Mouse IgG Reagent MP-6402-15
Anti-GFAP	Rabbit 1:400	Dako Z0334	ImmPRESS VR HRP Anti-Rabbit IgG Reagent MP-6401-15
Anti-GLUT	Rabbit 1:400	Abcam 131554	ImmPRESS VR HRP Anti-Rabbit IgG Reagent MP-6401-15
Anti-GABA	Rabbit 1:1000	ImmuSmol IS1006	ImmPRESS VR HRP Anti-Rabbit IgG Reagent MP-6401-15
Anti-Calbindin	Rabbit 1:5000	Swant CB38	ImmPRESS VR HRP Anti-Rabbit IgG Reagent MP-6401-15
Anti-Calretinin	Rabbit 1:5000	Swant 7697	ImmPRESS VR HRP Anti-Rabbit IgG Reagent MP-6401-15
UEA-I*	1:10	Vector L-1060	Rabbit 1:50 DAKO P289
LEA*	20 μg/ml	Vector B-1175	Vectastain ABC reagent PK-4000
BSI-B_4*	100 μg/ml	Sigma L-2140	Vectastain ABC reagent PK-4000
For double immunostaining of both Anti-Gαo (1:500) + Anti-Gαi2 (1:200), and Anti-MAP-2 (1:500) + Anti-Gαi2 (1:200) the first and second antibodies were the same as those used for the single immunostaining.			

Table 2: Sex differences in the volume of the rabbit AOB main layers (in μm^3). Data are expressed as Mean ± S.E.M.

	Males	Females
VNL	728,449,498 ± 71943802	761,912,023 ± 124,587,198
GlL	859,116,242 ± 129693385	786,005,578 ± 107,145,412
ECL	1,602,796,215 ± 124092624	1,677,138,884 ± 246,963,840
ICL	1,430,140,439 ± 111006803	1,503,304,648 ± 213,078,758

FIGURE LEGENDS

Fig. 1 VNS structures in the rabbit. **a** Mid-line sagittal section of the head of the rabbit showing the vomeronasal organ (VNO), the vomeronasal nerve (VNN) and the main olfactory bulb (MOB). **b** Sagittal histological section of the VNO, showing the vomeronasal neuroepithelium (asterisk), the cartilaginous capsule (VNC) and the branches of vomeronasal nerves leaving the organ dorsocaudally (arrowheads). **c** Amyelinic nerve branch of the VNN in the nasal septum (arrowheads). **d** Nissl-stained section of the olfactory bulb. MOB, main olfactory bulb; AOB, accessory olfactory bulb; VNN, vomeronasal nerve; VNC, vomeronasal cartilage; VNO, vomeronasal organ.

Fig 2 Dissection of the vomeronasal nerve (VNN) and the accessory olfactory bulb (AOB). **a** Lateral view of the left nasal mucosa and anterior brain. The VNN is followed from its origin in the VNO, but it disappears when approaching the ethmoidal cribriform plate (arrowhead). **b** Medial view of the right olfactory bulb. The VNN is dissected out from the medial surface of the MOB. **c** Dorsal view of both olfactory bulbs, showing the arrival of the VNNs (black arrows) to the AOBs (white arrows). **d** Rostro-medial view of the left VNN and AOB. FL, frontal lobe; MOB, main olfactory bulb; AOB, accessory olfactory bulb; VNN, vomeronasal nerve.

Fig 3 Nissl-stained sections of the AOB. **a** Sagittal section of the olfactory bulb (OB) through the central axis of the AOB. **b** Transverse section of the OB through the central axis of the AOB showing the rostral horn of the lateral ventricle (*). **c** Higher magnification of the inset from (a). **d** Higher magnification of the inset from (b), showing the medial arrival of the VNNs to the AOBs (arrowheads). **e-f** Nissl-stained sections of the AOB (e) and MOB (f) showing the correspondence between their layers. AOB, accessory olfactory bulb; MOB, main olfactory bulb; VNL, vomeronasal nerve layer; ONL, olfactory nerve layer; GlL; glomerular layer; ECL, external cellular layer; ICL, internal cellular layer; EPL, external plexiform layer; MCL, mitral cell layer; IPL, internal plexiform layer; GrL, granule cell layer; FL, frontal lobe; WM, white matter; a, anterior; p, posterior; d, dorsal; v, ventral; m, medial; l, lateral.

Fig 4 Nissl (a,b,d,e, g), Bielschowsky (c), and Tolivia (f,h) stained sections of AOB layers. **a** Glomeruli of the AOB showing the periglomerular (PG) cells (arrowheads) concentrated along the deeper segment of the glomeruli. **b** Glomeruli of the MOB, well delineated around their perimeters by PG cells (arrowheads). **c** Bielschowsky staining shows how the fibres of the VNN embrace clusters of AOB glomeruli. **d** Main cellular types in the ECL: Large principal, rounded and tufted**.** In any case they had mitral-like shape. **e.** Tufted cells of the ECL frequently appeared concentrated. **f** External cellular layer (ECL) of the AOB, defined by the PG cells of the GlL (arrowheads) and the ICL. The arrows indicate the axonal fibres projecting from the ECL that overlay the ICL. These fibres constitute the contribution of the

AOB to the dorsal peduncle of the lateral olfactory tract (dLOT). **g** Mitral cells of the MOB. **h** Higher magnification of the boxed area from D showing the principal cells of the ECL. VNL, vomeronasal nerve layer; GlL, glomerular layer; ECL, external cellular layer; ICL, internal cellular layer.

Fig 5 Bielschowsky-stained sagittal sections of the AOB. **a** Sagittal section of the olfactory bulbs through the rostro-caudal axis of the AOB, showing its shape and layers, as well as the intrabulbar fibres (IBF) of the MOB. **b** Paramedian sagittal section of the OB, located laterally to the section displayed in (a), showing the main tracts of the bulb, the dorsal lateral olfactory tract (dLOT), ventral lateral olfactory tract (vLOT) and the rostral migratory stream (RMS). **c** Higher magnification of the inset from (a), showing the deeper layers of the AOB. The arrowheads show the myelinic fibres projecting from the external cellular layer (ECL), which constitute the contribution of the AOB to the dLOT. FL, frontal lobe; AOB, accessory olfactory bulb; MOB, main olfactory bulb; IBF, intrabulbar fibres; dLOT, dorsal lateral olfactory tract; RMS, rostral migratory stream; vLOT, ventral lateral olfactory tract; LV: rostral horn of the lateral ventricle; ECL, external cellular layer; ICL, internal cellular layer.

Fig 6 Immunostaining for GFAP and OMP in the AOB. **a** Anti-GFAP staining was restricted to the VNL in the AOB. Additionally, there was a definite area of immunolabelling around the periphery of the AOB (arrows). **b** Higher magnification of the superior inset showed from (a) confirms the immunostaining of the processes of the vomeronasal ensheathing cells in the AOB neuropil. **c** Occasionally, the cell bodies of the ensheathing cells were discernible. **d** Higher magnification of the inferior inset from (a) shows a conspicuous presence of astrocytes external to the pial basement membrane that surrounds the AOB. **e** Anti-OMP uniformly stains both superficial layers of the AOB: the VNL and the GlL. **f** The anti-OMP immunolabelling also labels the corresponding layers of the MOB: the ONL and the GlL. GFAP, glial fibrillary acidic protein; OMP, olfactory marker protein; VNL, vomeronasal nerve layer; GlL, glomerular layer; ONL, olfactory nerve layer.

Fig 7 Immunohistochemical labelling of the G proteins subunits and GAP-43 and the lectin histochemical labelling of the OBs. **a** Double immunostaining for Gαi2 and Gαo in the AOB. Anti-Gαi2 (brown) stains the anterior half of the VNL and GlL of the AOB. Anti-Gαo (red) stains the posterior half of the VNL and GlL. **b** Single immunostaining with anti-Gαo showing glomeruli in the anterior half of the AOB that are partially stained. This labelling corresponds with the dendrites from neurons in the underlying layers of the AOB. **c** Simple immunolabelling with anti-Gαi2 stains the anterior VNL and GlL of the AOB. The posterior zone is devoid of labelling. **d** Simple immunolabelling with anti-Gαo stains the complementary posterior half of the VNL and GlL of the AOB. The anterior half of the VNL layer is not stained. As observed in (b), some glomeruli in the anterior half are stained. **e** LEA histochemical labelling of the AOB labels both vomeronasal axons and glomeruli in the whole AOB. **f** AOB immunostaining with anti-GAP-43

labels the superficial layer and the ICL. In the superficial layer anti-GAP43 labelling reveals an antero-posterior zonation. In the ECL, anti-GAP43 establishes a distinction between the presumptive EPL (1) and IPL (2). **g** BSI-B_4 histochemical labelling of the AOB, produces a similar pattern as that observed with LEA labelling, staining the superficial layers of the whole AOB. **h** MOB immunostaining with anti-GAP-43 produces a pattern similar to that shown in (f) for the AOB, confirming the neat distinction between the EPL and the IPL. a, anterior; p, posterior; ICL, internal cellular layer; EPL, external plexiform layer; IPL, internal plexiform layer; VNL, vomeronasal nerve layer; GlL, glomerular layer.

Fig 8 Immunohistochemical labelling of MAP-2 and GLS in the OBs. **a** Double immunostaining with MAP-2 and Gαi2 antibodies in the AOB. Anti-MAP-2 (red) profusely stains the dendritic trees of principal/mitral cells of the AOB/MOB respectively and granular cells in both OBs, as well as the pyramidal cells in the frontal lobe (FL). **b** Higher magnification of the inset depicted in (a), showing the AOB layers. The contributions of both vomeronasal axons (brown) and principal cell dendritic trees to the glomeruli of the AOB (asterisks) are noticeable. The soma of the principal cells and the axons contributing to the dorsal peduncle of the lateral olfactory tract remain unlabelled (black arrowheads). The spherical cell bodies and processes of granule cells are immunolabelled (white arrowheads). **c** The mitral cells of the MCL layer of the MOB are immunopositive to anti-GLS. **d** Principal cells in the ECL of the AOB immunostained with anti-GLS. Both large principal (black arrowheads) and tufted cells (white arrowheads) are immunopositive. MAP-2, microtubule-associated protein 2; GLS, glutaminase; FL, frontal lobe; LOT, lateral olfactory tract; a, anterior; p, posterior; VNL, vomeronasal nerve layer; ECL, external cellular layer; ICL, internal cellular layer; MCL, mitral cellular layer.

Fig 9 Immunohistochemical labelling of calcium-binding proteins in the OBs. **a** Low-power sagittal section of the AOB immunostained with the antibody against CR. The superficial and middle layers show intense labelling of their neuropils. This staining appears to be stronger in the VNL and GlL. **b** AOB immunostained with anti-CB shows a pattern similar to that for anti-CR immunostaining. **c** The only cellular elements immunostained in the AOB are concentrated in the ICL, where the granule cells and their processes are stained by anti-CR. **d** In the MOB, anti-CR stains both the PG and granular cells, whereas CB immunostaining (**e**) labels only the PG cells. VNL, vomeronasal nerve layer; GlL, glomerular layer; ECL, external cellular layer; ICL, internal cellular layer; CB, calbindin; CR, calretinin.

Fig 10 Drawings of the olfactory bulbs, showing the topographical organisation of the four neuronal clusters identified in the accessory bulbar core white matter. **a** The α and β groups are located parallel to the caudal half of the bulb, whereas the γ and δ groups are beneath the rostral third of the bulb. **b** Schematic drawing of the topographic relationships between the nuclei and the AOB: α (green), β (dark blue), γ (red), and δ (light blue). **c** Rostro-ventral view of the rabbit brain, showing the area depicted in

(a). AOB, accessory olfactory bulb; MOB, main olfactory bulb; FL, frontal lobe; dLOT, dorsal lateral olfactory tract; vLOT, ventral lateral olfactory tract

Fig 11 Three selected photomicrographs of the Nissl-stained sagittal serial sections of the AOB, showing the four neuronal clusters present in the accessory bulbar core white matter. The sections are ordered from medial (**a**) to lateral (**c**). **d-g** Higher magnifications of the four nuclei shown in a-c: γ (d), α (e), β (f), and δ (g). a, anterior; p, posterior; d, dorsal; v, ventral. Scale bars: a-c, 250 μm; d-g 100 μm

Fig 12 Histological and immunohistochemical study of the intrabulbar neuronal clusters. **a** Low-power photomicrograph of the Nissl-stained γ group. **b** Higher magnification of the inset from (a), showing the cellular organisation of the nucleus. **c** Bielschovsky-stained, pyronin-counterstained, sagittal section of the α group. **d** Bielschovsky-stained section of the α group. **e** Anti-GLS immunohistochemical labelling of the α and γ groups. a, anterior; p, posterior; d, dorsal; v, ventral; GLS, glutaminase. Scale bars: a, 500 μm; b, d, 100 μm; c, 50 μm; e, 250 μm

Fig 13 Four selected photomicrographs of Nissl-stained transverse serial sections of the AOB, containing the four neuronal clusters of the accessory bulbar core white matter. The sections are ordered from caudal (**a**) to rostral (**d**). **e-h** Higher magnifications of the four nuclei shown in A-D: β (e), α (f), δ (g), and γ (h). m, medial; l, lateral; d, dorsal; v, ventral; *, vomeronasal nerve. Scale bars: a-d, 1 mm; e-h, 50 μm

Fig 14 Morphometric study of the AOB layers volume sexual dimorphism. There were not statistically significant sexual differences. Unpaired Student's t test. Data are mean ± s.e.m.; n = 6 rabbits per sex. VNL, Vomeronasal nerve layer; GIL Glomerular layer; ECL, External cellular layer; ICL, Internal celular layer.

Fig 15 Stereological study of the sexual dimorphism in the numeric cell density of the principal cells of the ECL layer of the AOB. There were statistically significant sexual differences. Data are mean ± s.e.m.. Unpaired Student's t test. n = 6 rabbits per sex. *** $p<0.01$

SUPPLEMENTARY FIGURE LEGENDS

Suppl. Fig. S1 Morphometric study of the volume of the MOB layers comparing both sex. There were not statistically significant sexual differences unless in the deep ICL. Unpaired Student's t test. Data are mean ± s.e.m.; n = 6 rabbits per sex. * $p<0.05$. ONL, Olfactory nerve layer; GlL Glomerular layer; MPL, Mitral cell + Plexiform layers; eGrL, External granule cell layer; iGrL, Internal granule cell layer.

Suppl. Fig. S2 Anti GABA immunolabelling of the rabbit AOB. A, Immunopositive periglomerular cells (arrows). B, Haematoxylin counterstained section of the ICL showing immunopositive granule cells.

Suppl. Fig. S3: Morphometric analysis of the female AOB: layers volume quantification using ImageJ. Each layer has been outlined and filled by a pseudocolor (grayscale) following a constant pattern. The numbers indicate the different layers: 1, vomeronasal nerve layer (VNL); 2, glomerular layer (GlL); 3, external cellular layer (ECL); 4, internal cellular layer (ICL). The experiment was blinded by using the codes in the figures. The real animals were the following: bird=female1; mouse=female2; cat=female3; dog=female4; cow=female5; horse=female6.

Suppl. Fig. S4: Morphometric analysis of the male AOB: layers volume quantification using ImageJ. Each layer has been outlined and filled by a pseudocolor (grayscale) following a constant pattern. The numbers indicate the different layers: 1, vomeronasal nerve layer (VNL); 2, glomerular layer (GlL); 3, external cellular layer (ECL); 4, internal cellular layer (ICL). The experiment was blinded by using the codes in the figures. The real animals were the following: deer=male1; penguin=male2; pig=male3; rat=male4; lion=male5; tiger=male6.

Suppl. Fig. S5: Morphometric analysis of the female MOB: layers volume quantification using ImageJ. Each layer has been outlined and filled by a pseudocolor (grayscale) following a constant pattern. The numbers indicate the different layers: 1, accessory olfactory bulb (AOB); 2, vomeronasal nerve layer (VNL); 3, glomerular layer (GlL); 4, external cellular layer (ECL); 5, external granular layer (eGrL); 6, internal granular layer (iGrL); 7, white matter (WM); 8, third ventricle (3V). The experiment was blinded by using the codes in the figures. The real animals were the following: red=female1; blue=female2; purple=female3; yellow=female4; brown=female5; white=female6.

Suppl. Fig. S6: Morphometric analysis of the male MOB: layers volume quantification using ImageJ. Each layer has been outlined and filled by a pseudocolor (grayscale) following a constant pattern. The numbers indicate the different layers: 1, accessory olfactory bulb (AOB); 2, vomeronasal nerve layer

(VNL); 3, glomerular layer (GlL); 4, external cellular layer (ECL);); 5, superficial granular layer (SGrL); 6, Deep granular layer (DGrL); 7, white matter (WM); 8, third ventricle (3V). The experiment was blinded by using the codes in the figures. The real animals were the following: orange=male1; pink=male2; grey=male3; black=male4; green=male5; maroon=male6.

Suppl. Fig. S7: Figures made up of several photographs by merging them with the image-stitching software (PTGui Pro). The resulting mosaics are presented as follow: Red lines round the pictures taken of transversal sections of the OB. a β cluster; b α cluster; c δ cluster; γ cluster (see Fig 13a-d in the manuscript).

Suppl. Fig. S8: Figures made up of several photographs by merging them with the image-stitching software (PTGui Pro). The resulting mosaics are presented as follow: Red lines round the pictures taken of sagittal sections of the OB. a Nissl staining (see Fig 12a-d in the manuscript); b and c Bielschowsky staining (see Fig 5a,b in the manuscript).

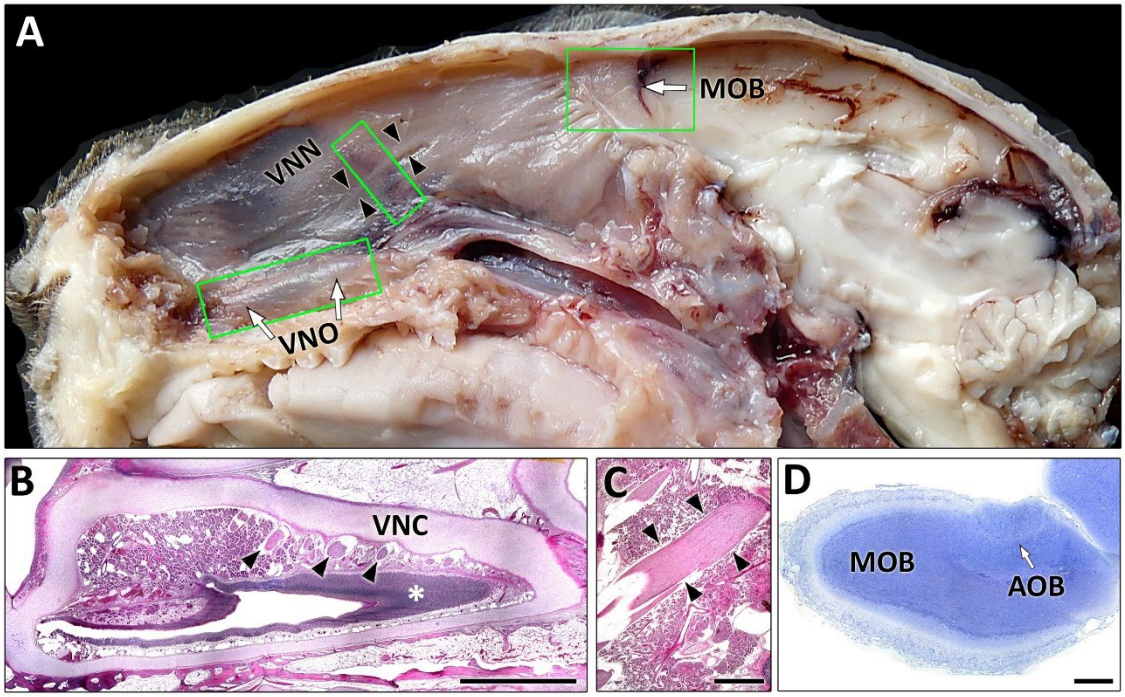

1209

1210 **Figure 1**

1211

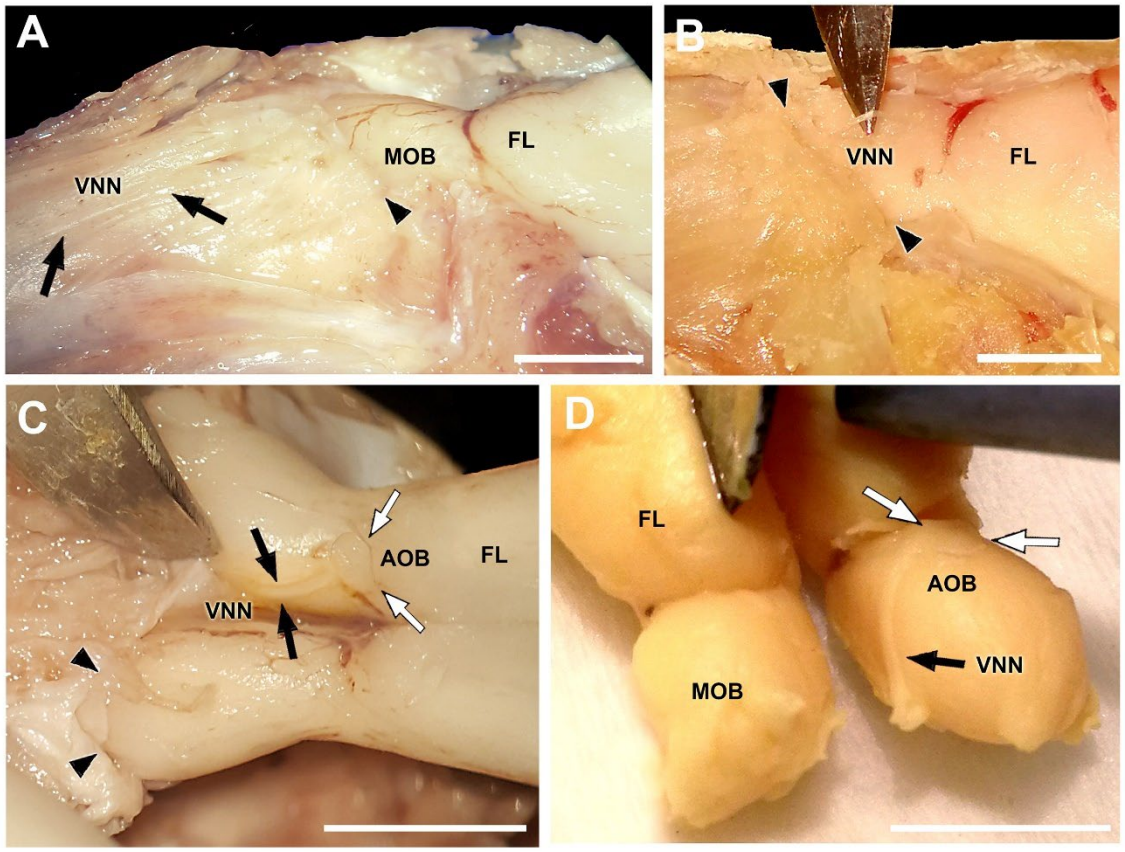

1212

1213 **Figure 2**

1214

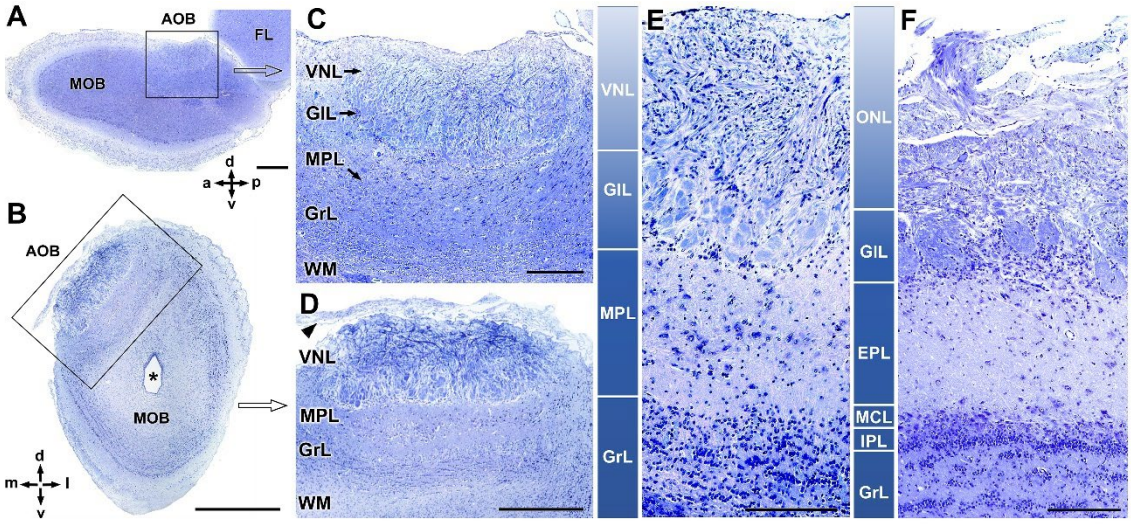

Figure 3

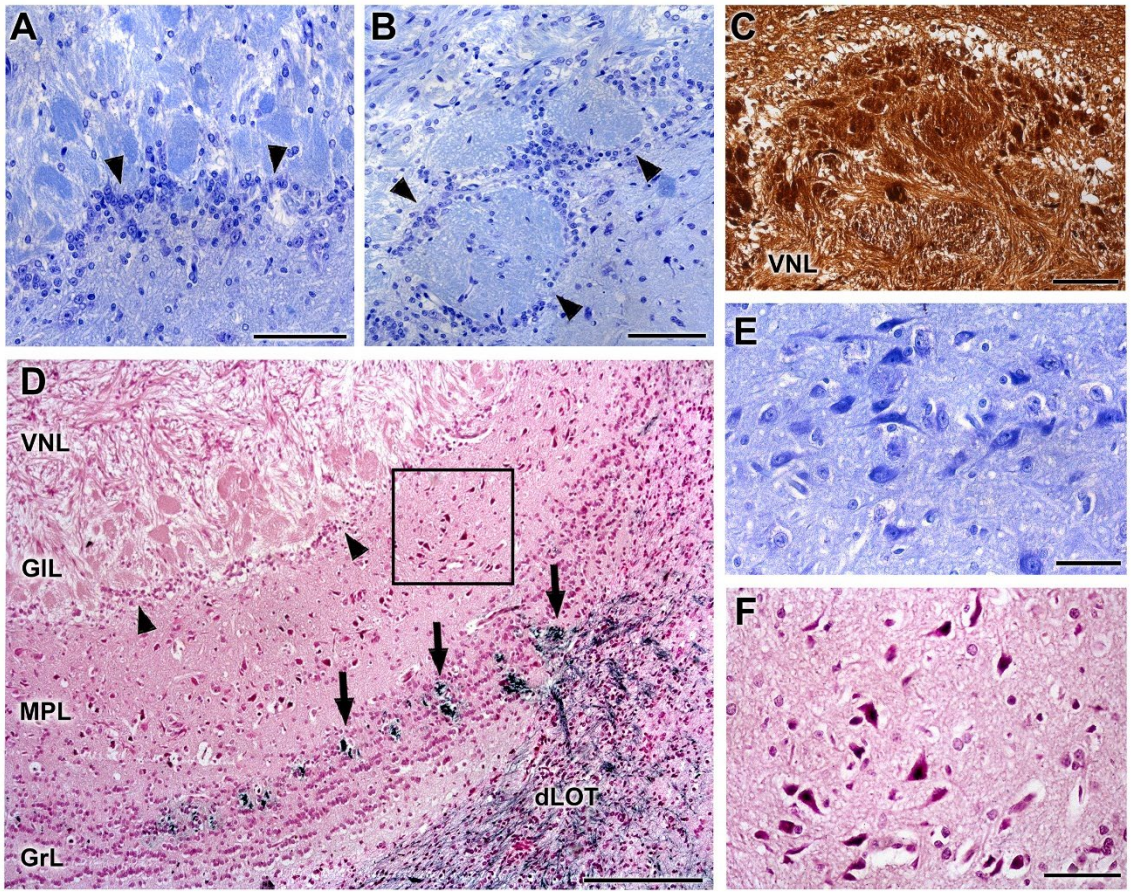

Figure 4

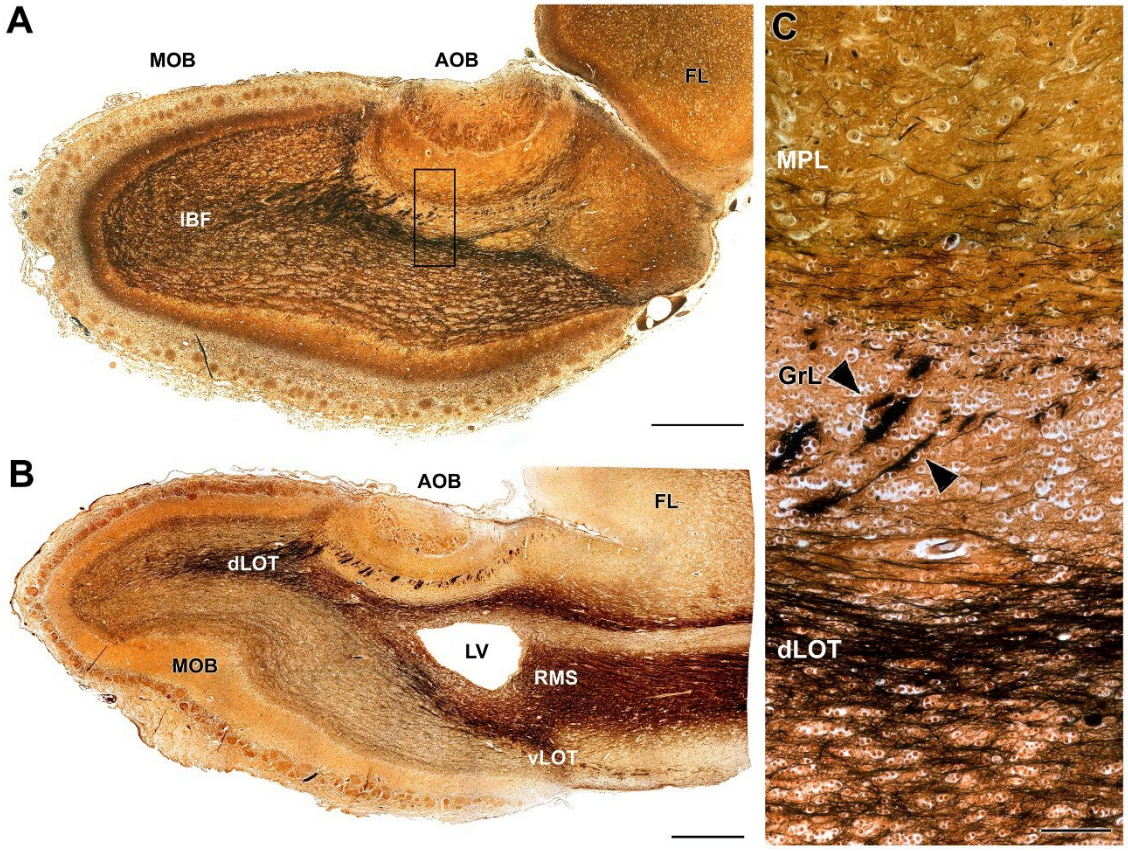

1223

1224 **Figure 5**

1225

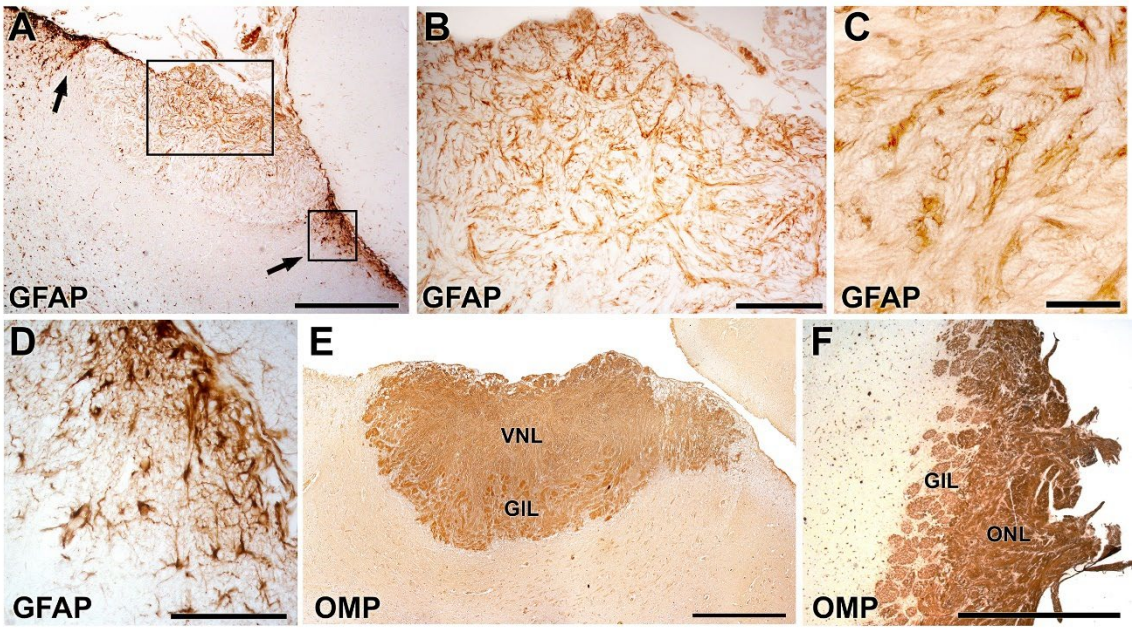

1226

1227 **Figure 6**

1228

1229

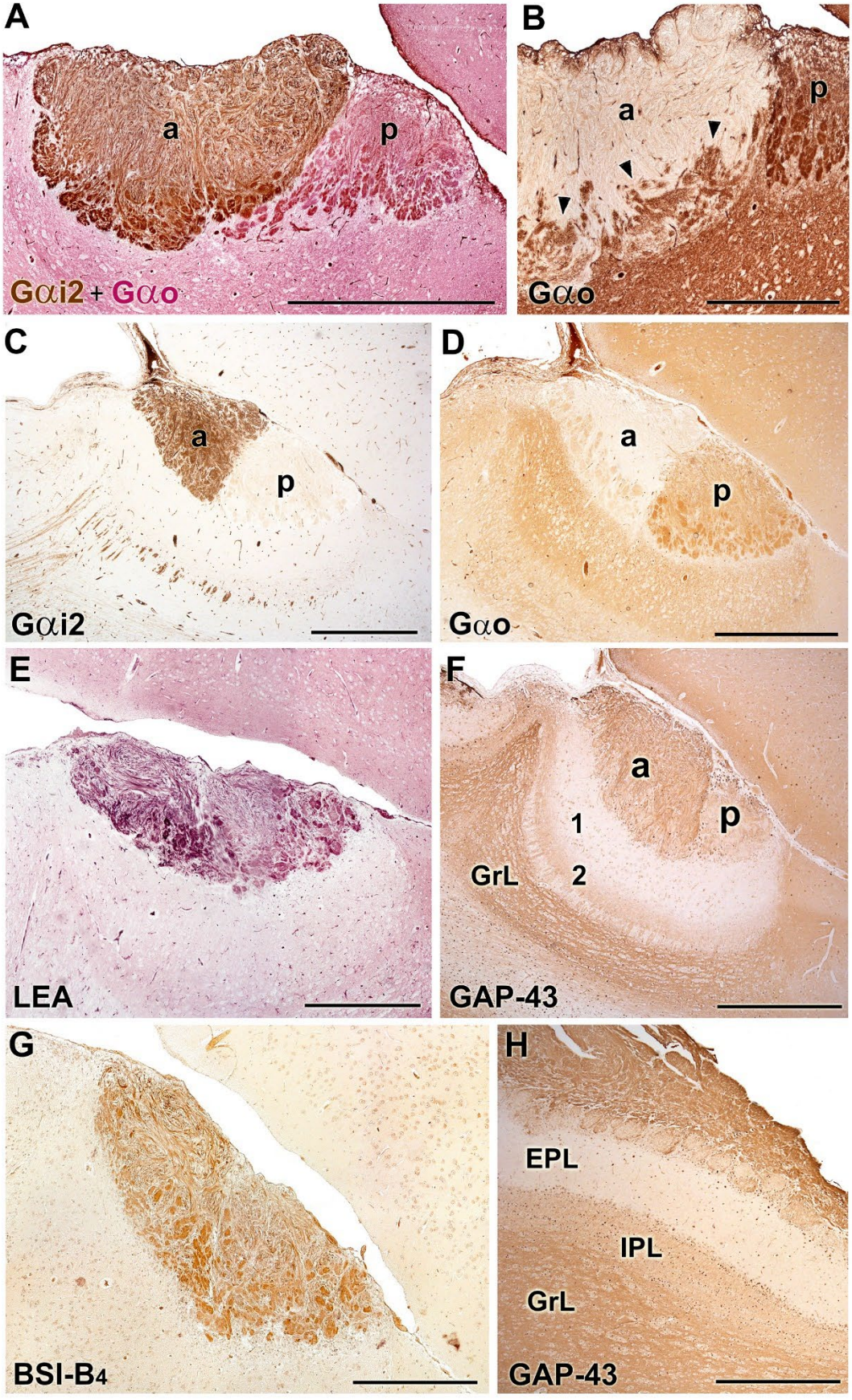

1230

1231

Figure 7

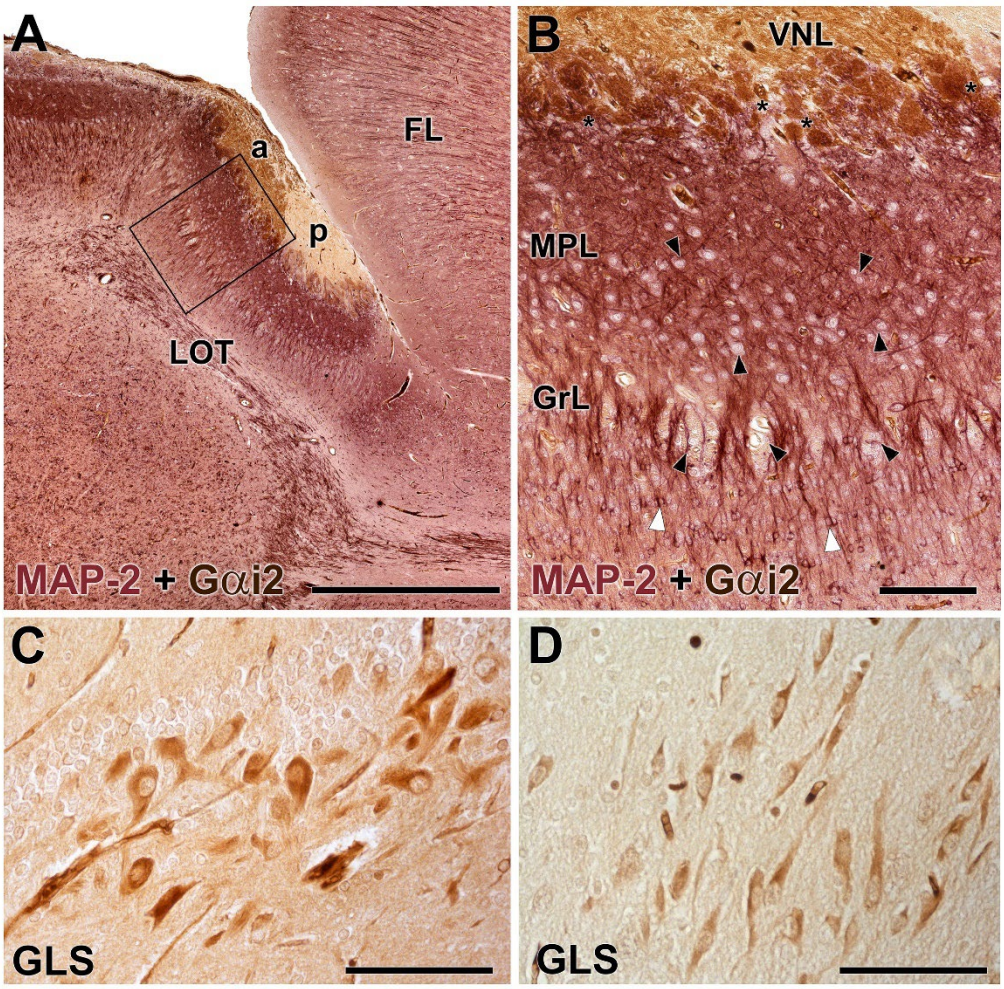

1232

1233 **Figure 8**

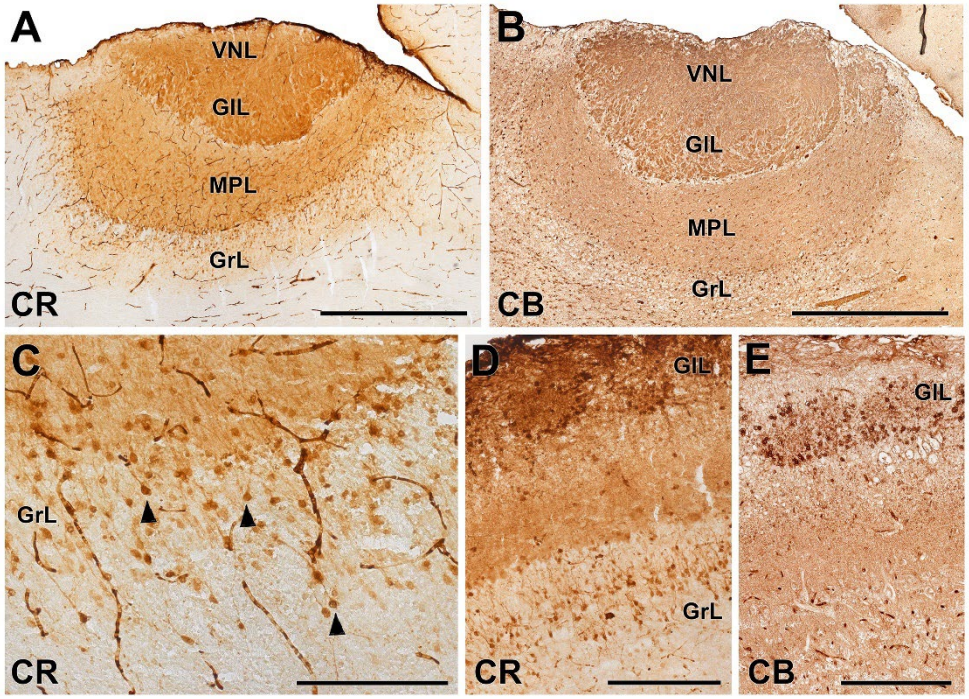

1234

1235 **Figure 9**

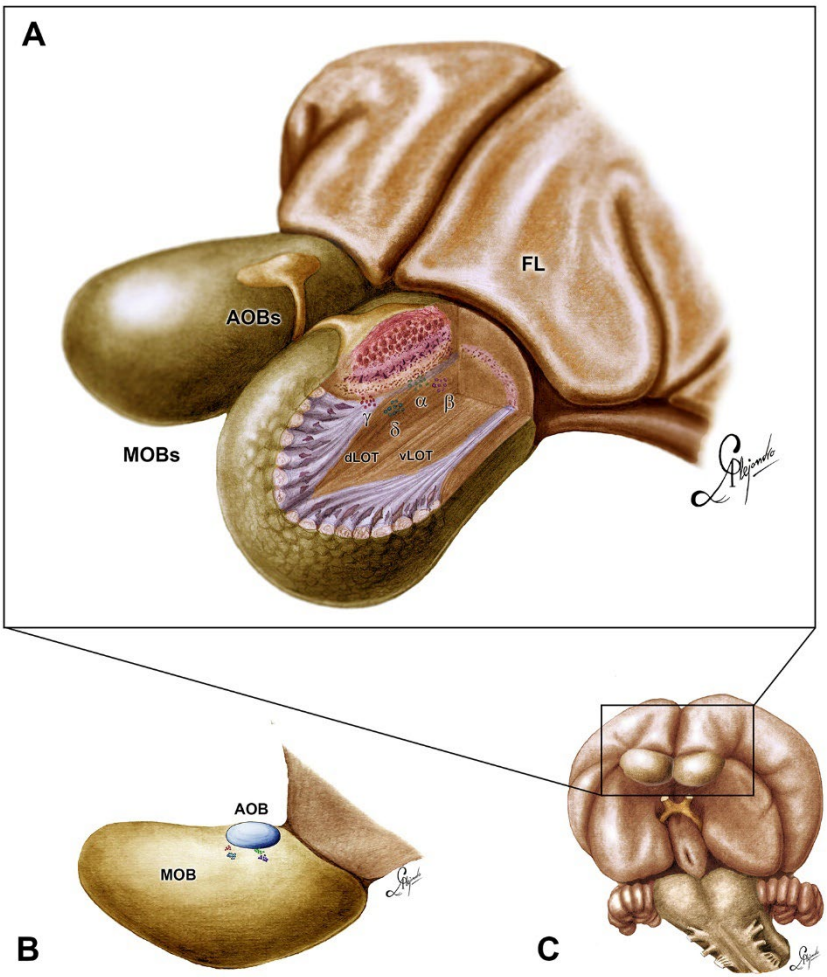

1236

1237 **Figure 10**

1238

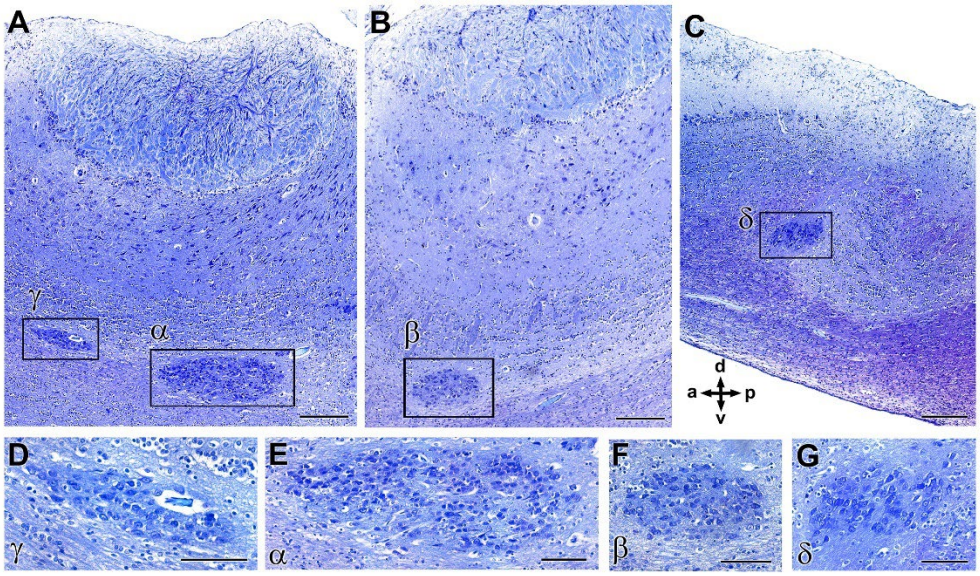

1239

1240 **Figure 11**

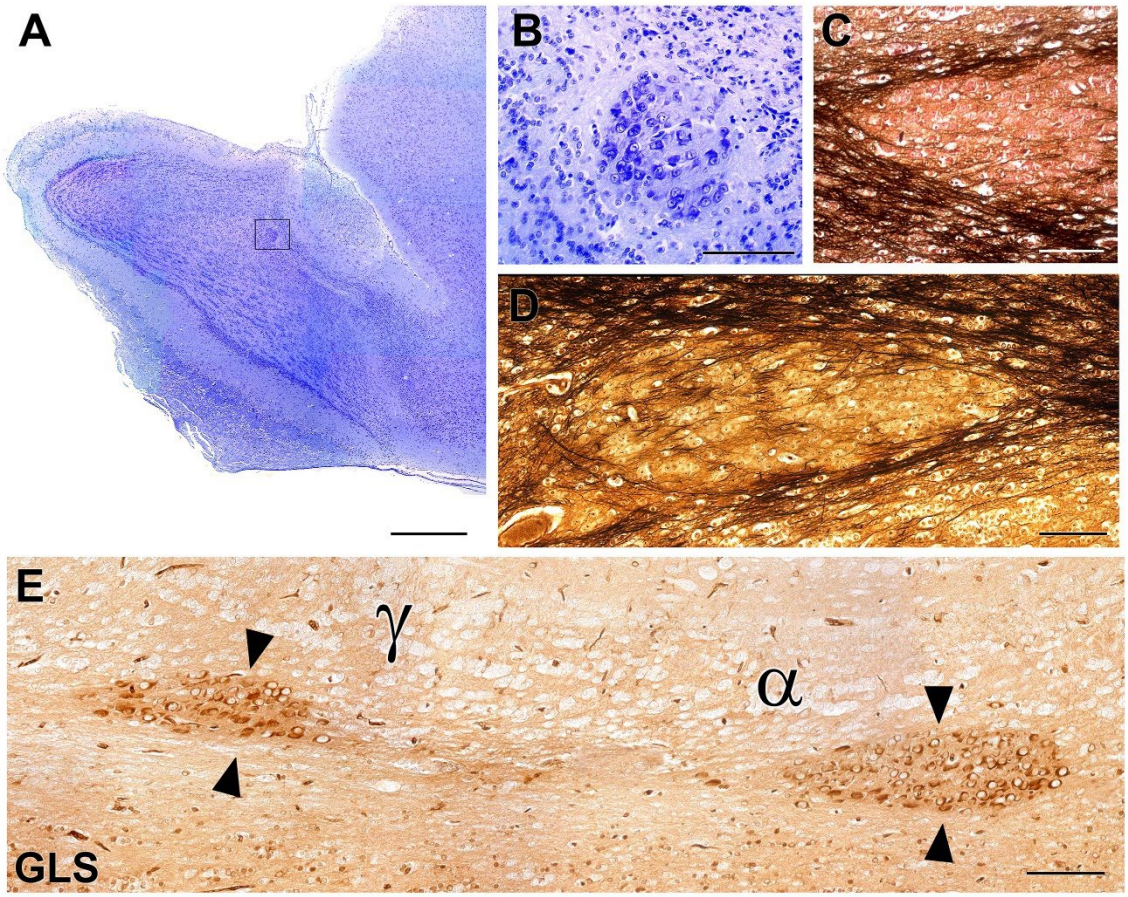

1241

1242 **Figure 12**

1243

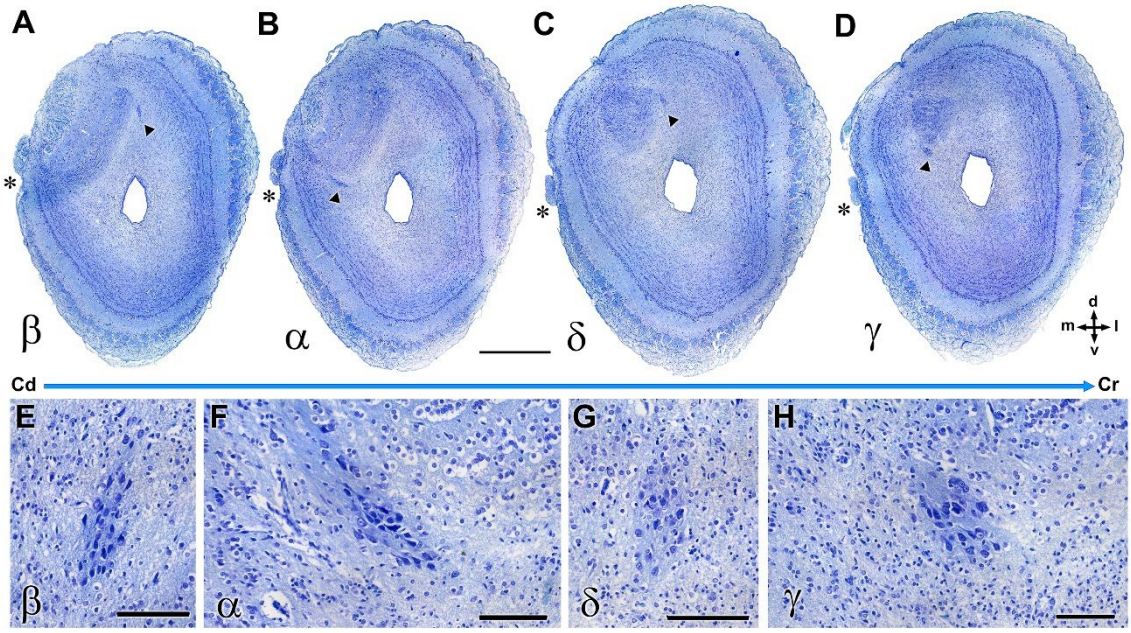

1244

1245 **Figure 13**

1246

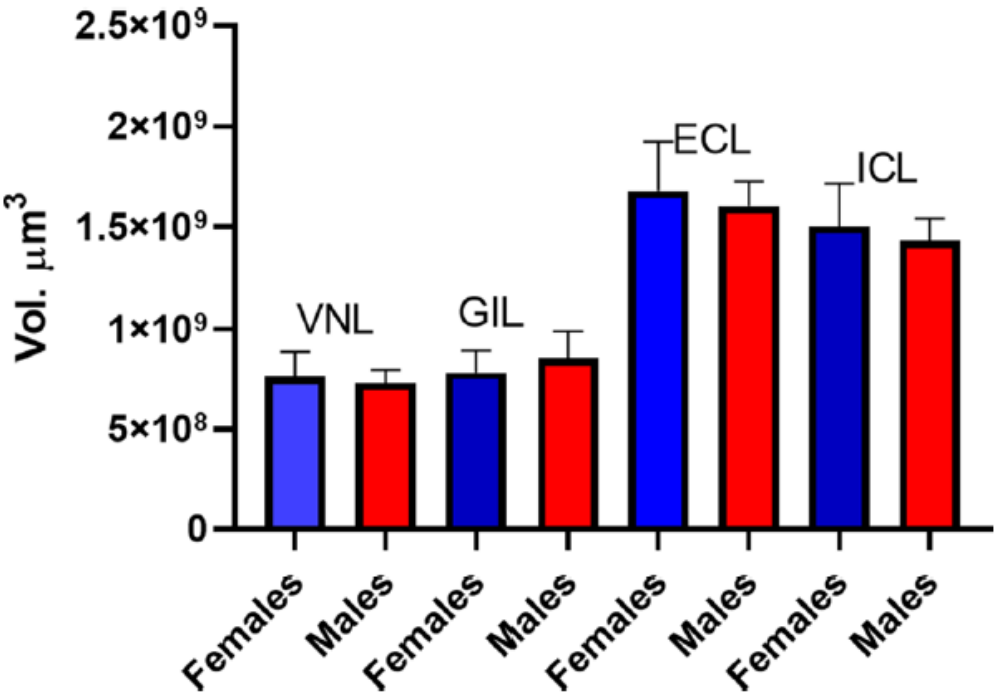

1247

1248 **Figure 14**

1249

1250

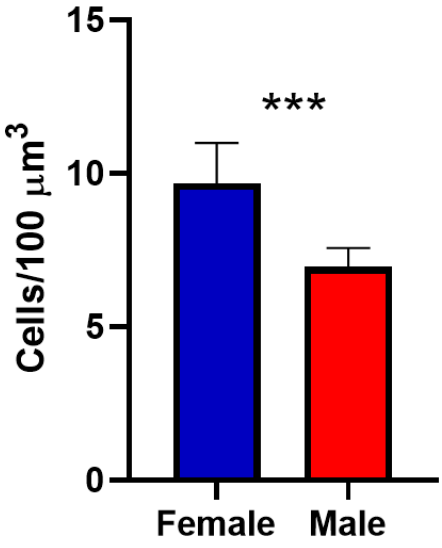

1251

1252 **Figure 15**

1253

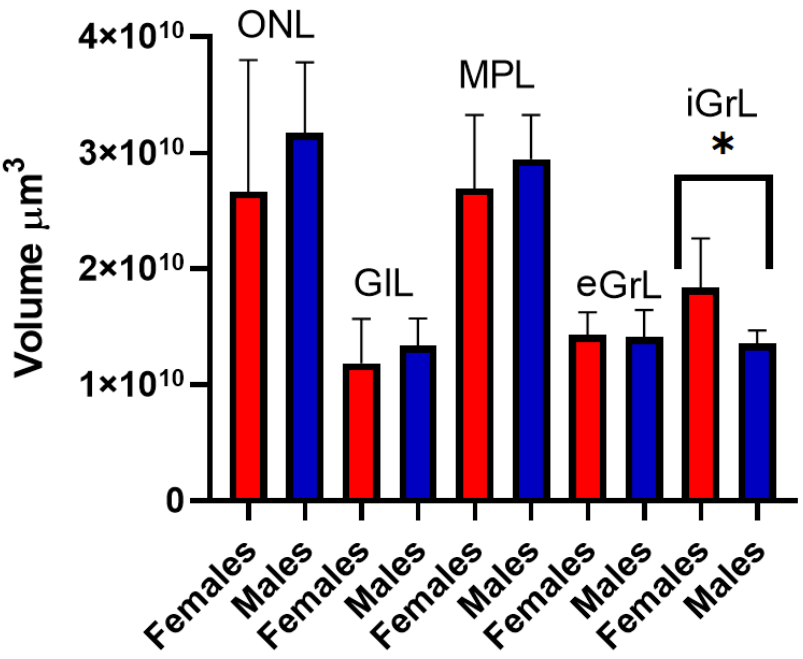

Suppl. Fig. 1

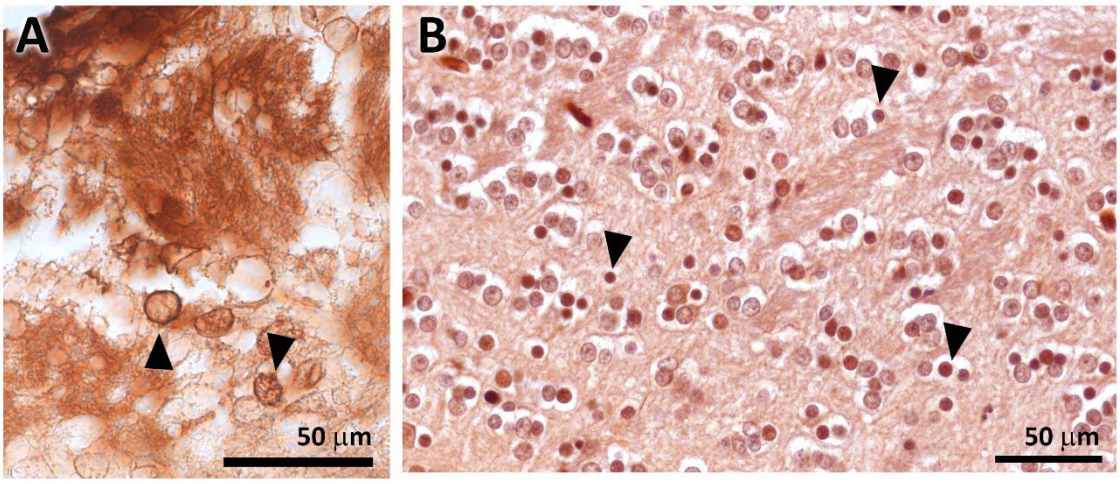

Suppl. Fig. 2

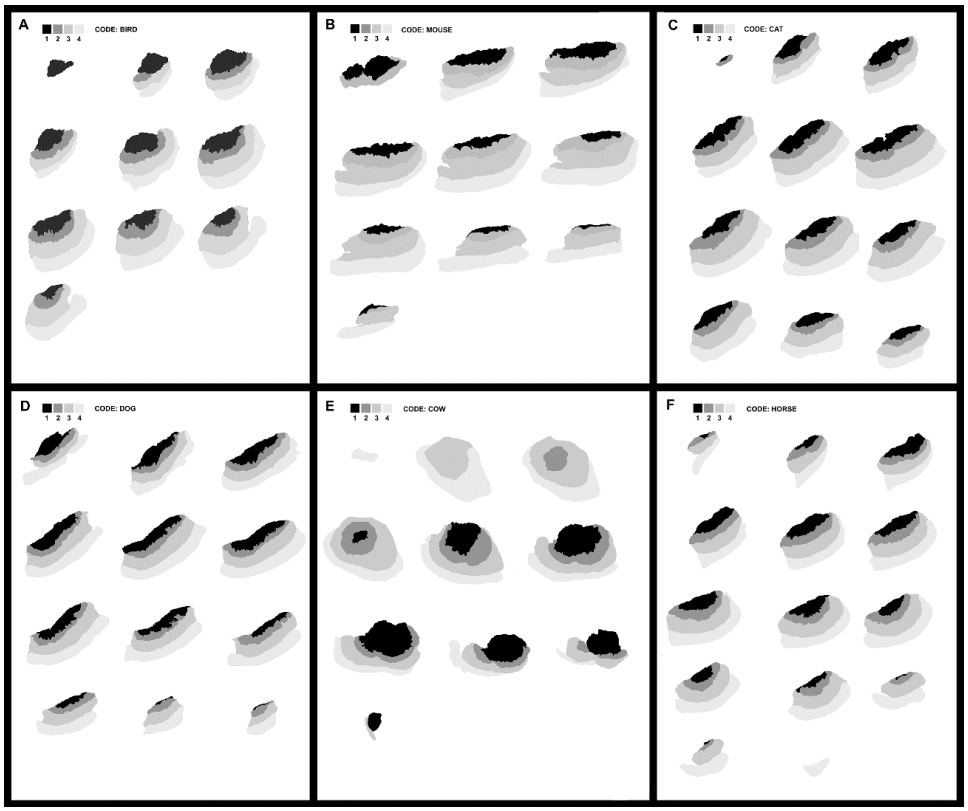

Suppl. Fig. 3

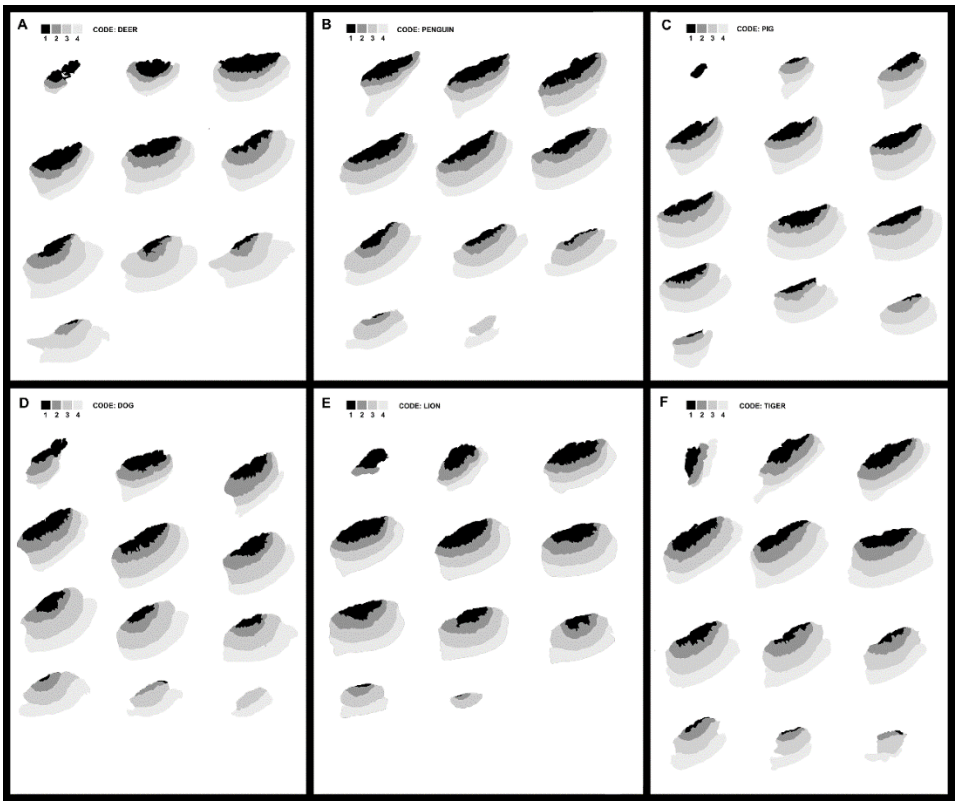

Suppl. Fig. 4

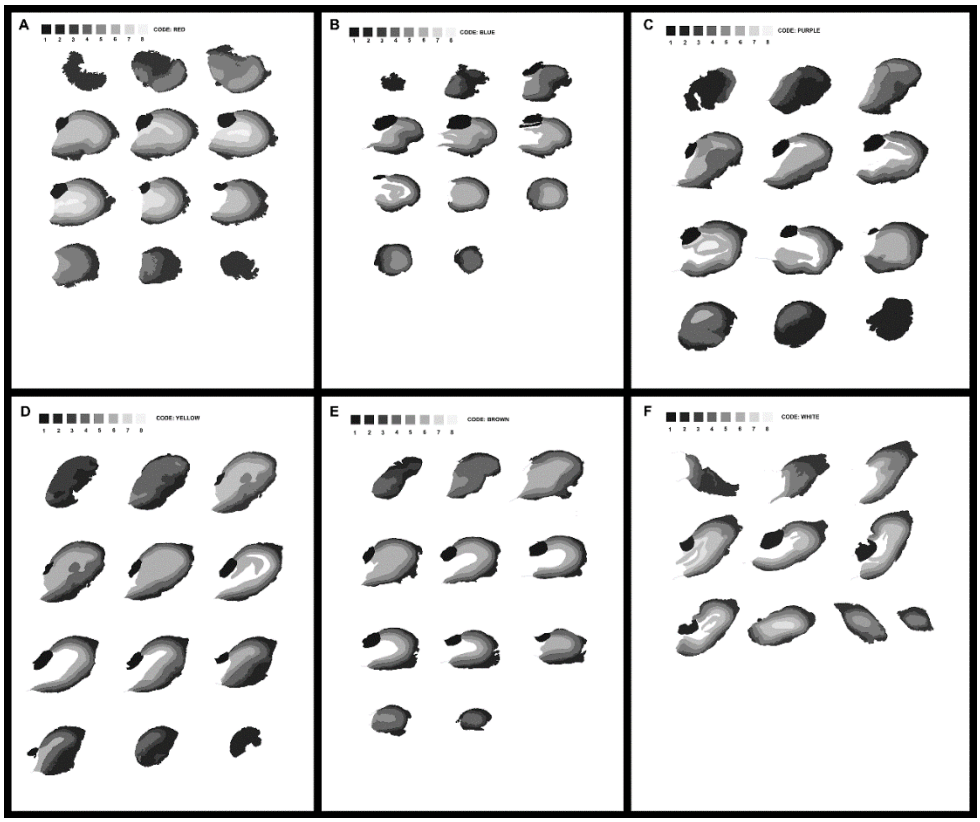

Suppl. Fig. 5

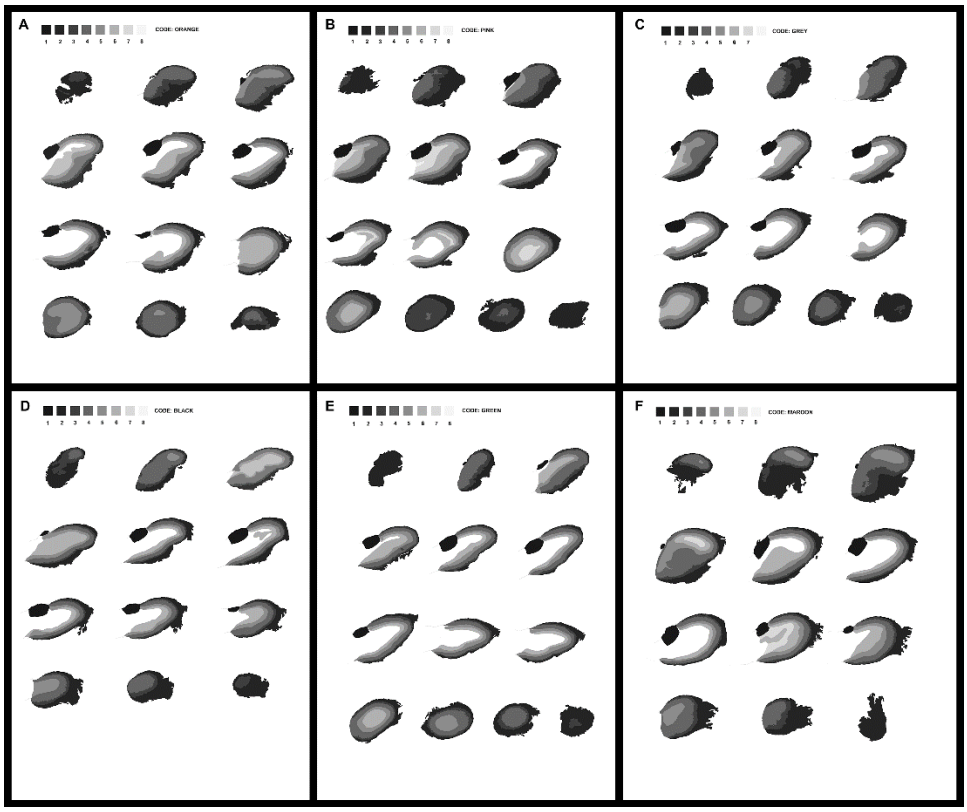

Suppl. Fig. 6

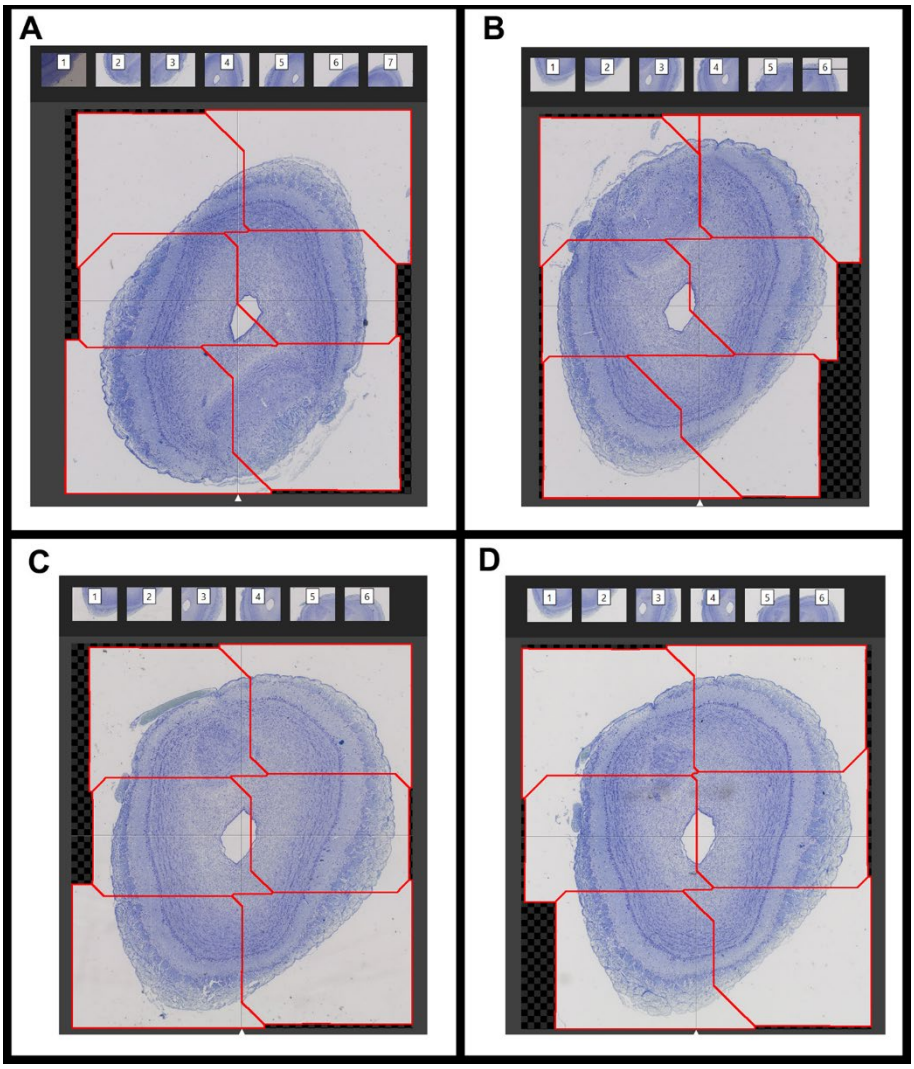

Suppl. Fig. 7

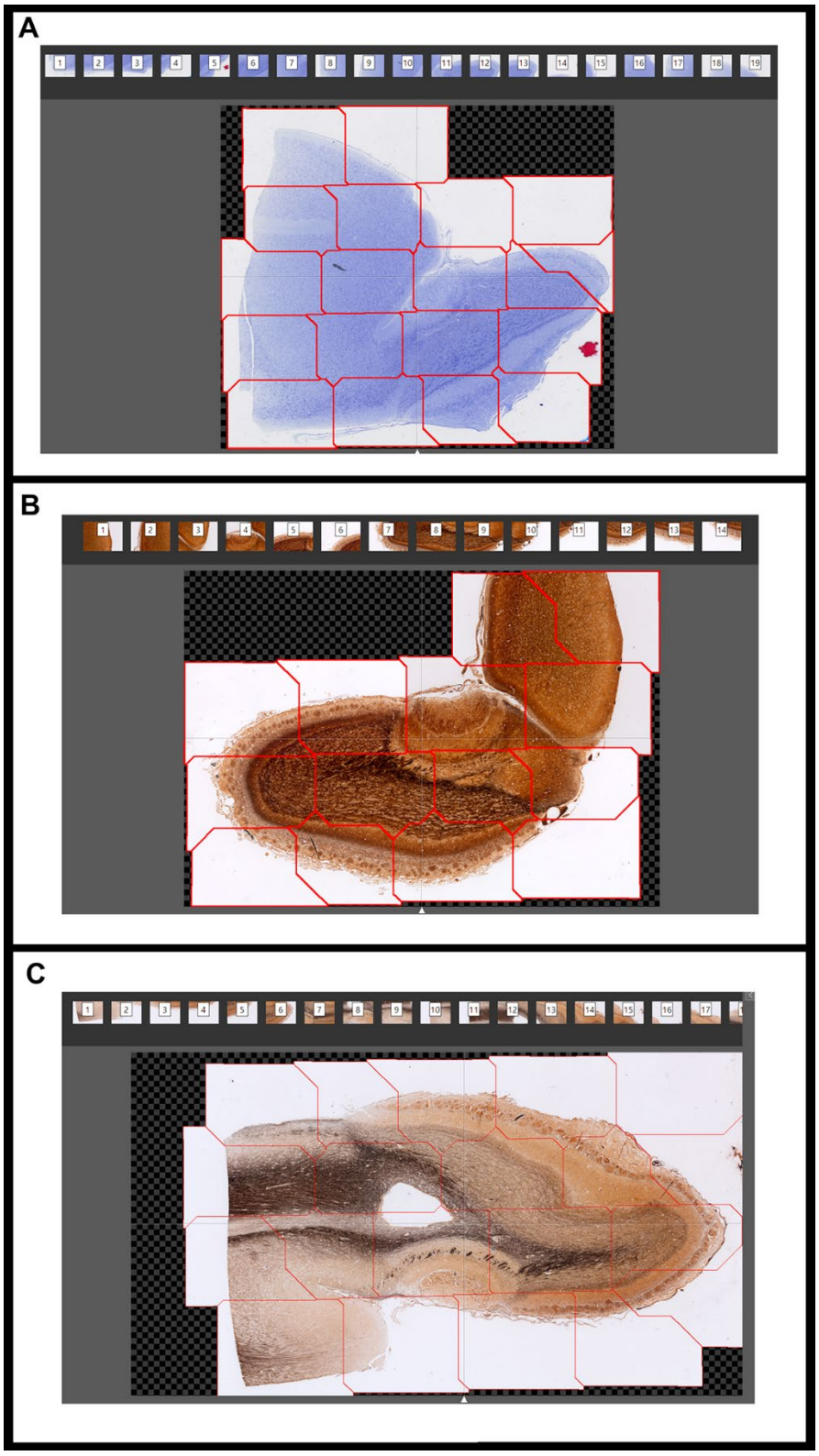

Suppl. Fig. 8